AGU PUBLICATIONS

JGR

Journal of Geophysical Research: Atmospheres

RESEARCH ARTICLE
10.1002/2015JD023298

Key Points:
- Black carbon shows opposite seasonal cycle in the lower and free troposphere
- The seasonal cycle of BC is driven mainly by seasonal changes in meteorology
- Regional transport significantly impact BC distribution

Supporting Information:
- Supporting Information S1
- Figure S1
- Figure S2

Correspondence to:
R. Kumar,
rkumar@ucar.edu

Citation:
Kumar, R., M. C. Barth, G. G. Pfister, V. S. Nair, S. D. Ghude, and N. Ojha (2015), What controls the seasonal cycle of black carbon aerosols in India?, *J. Geophys. Res. Atmos.*, *120*, 7788–7812, doi:10.1002/2015JD023298.

Received 24 FEB 2015
Accepted 12 JUL 2015
Accepted article online 16 JUL 2015
Published online 10 AUG 2015

What controls the seasonal cycle of black carbon aerosols in India?

Rajesh Kumar[1,2], M. C. Barth[2], G. G. Pfister[2], V. S. Nair[3], Sachin D. Ghude[4], and N. Ojha[5]

[1]Advanced Study Program, National Center for Atmospheric Research, Boulder, Colorado, USA, [2]Atmospheric Chemistry Division, National Center for Atmospheric Research, Boulder, Colorado, USA, [3]Space Physical Laboratory, Vikram Sarabhai Space Center, Thiruvanantpuram, India, [4]Indian Institute of Tropical Meteorology, Pune, India, [5]Atmospheric Chemistry Department, Max Planck Institute for Chemistry, Mainz, Germany

Abstract The seasonal variability of black carbon (BC) aerosols in India is studied using high resolution (10 km) BC simulations conducted using the Weather Research and Forecasting Model coupled with Chemistry. The model reproduces the observed seasonality of surface BC fairly well over most parts of India but fails to capture the seasonality in the Himalayas and deviates from the observed BC magnitude at several sites. The errors in modeled BC are attributed to uncertainties in BC emissions and their diurnal cycle, planetary boundary layer height underestimation, and aerosol processes. Model results show distinct but opposite seasonality of BC in the lower (LT) and free troposphere (FT) with BC showing winter maximum and summer minimum in the LT and vice versa in the FT. Our analysis shows that BC seasonality is not driven by seasonality of the anthropogenic emissions but by changes in the regional meteorology through weakening of the horizontal transport and strengthening of the vertical transport of BC during summertime compared to winter. BC in both the LT and FT comes mostly from anthropogenic emissions followed by biomass burning emissions except during winter when long-distant sources become more important in the FT. BC in the FT is significantly affected by anthropogenic emissions from all parts of India. The source-receptor relationship changes seasonally, but the regional transport remains a significant contributor to BC loadings in the LT of India, highlighting the necessity of considering nonlocal sources along with local emissions when designing strategies for mitigating BC impacts on air quality.

1. Introduction

The interest in black carbon (BC) aerosols has grown rapidly over the recent decades because of the ability of BC to strongly absorb incoming solar radiation and thereby affect the Earth's climate system [e.g., *Jacobson*, 2001; *Ramanathan and Carmichael*, 2008; *Bond et al.*, 2013; *Surendran et al.*, 2013], atmospheric thermodynamics [e.g., *Satheesh and Ramanathan*, 2000; *Menon et al.*, 2002], lifetime and optical properties of clouds [e.g., *Hansen et al.*, 1997; *Koch and Del Genio*, 2010], and freshwater resources [e.g., *Menon et al.*, 2002, 2010; *Jacobson*, 2004; *Lau et al.*, 2006; *Lau and Kim*, 2010; *Yasunari et al.*, 2010]. In addition, BC-containing particles are also suggested to adversely affect human health [e.g., *Dockery and Stone*, 2007; *Janseen et al.*, 2012], lower crop yields [e.g., *Chameides et al.*, 1999], and adversely affect terrestrial and aquatic ecosystems [e.g., *Forbes et al.*, 2006]. To better assess the magnitude of these effects of BC, we need to understand seasonal variations of BC. The knowledge of seasonal cycle of BC at the surface will help identify the periods when human health and ecosystems are at a greater risk due to BC pollution, while such a knowledge for the free troposphere and atmospheric column will help us better understand the implications of BC aerosols for the climate, atmospheric circulation, and the hydrological cycle.

BC is a by-product of incomplete combustion and is emitted from a variety of anthropogenic (industries, automobiles, power plants, domestic cooking and heating, and agricultural residue burning) and biomass burning (forests and savannas) sources [e.g., *Bond et al.*, 2007, 2013]. The total global emissions of BC aerosols estimated from bottom-up approaches are reported to be 7500 Gg yr^{-1} for the year 2000 but with a large uncertainty range of 2000–29000 Gg yr^{-1} [*Bond et al.*, 2013]. BC particles are almost chemically inert under atmospheric conditions and are removed from the atmosphere primarily by wet and dry deposition at the surface with the former representing 70–85% of the total loss globally [*Pöschl*, 2005]. The average atmospheric lifetime of BC particles is about 1 week [*Bond et al.*, 2013], enabling it to undergo regional and intercontinental transport and making it a potential candidate for short-term global warming mitigation [*Ramanathan and Carmichael*, 2008].

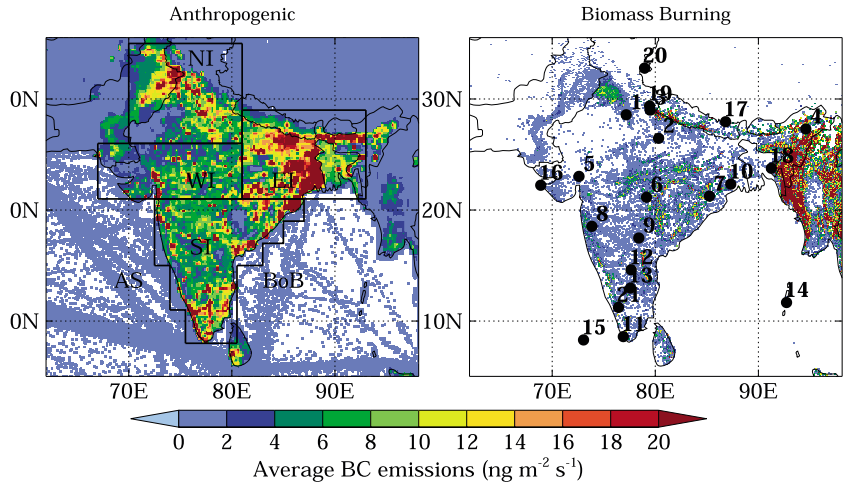

Figure 1. Annual average anthropogenic and biomass burning emissions of BC over the model domain for the year 2011. White spaces represent areas of zero BC emissions. Different regions from which anthropogenic BC emissions are tagged are shown with the Bay of Bengal (BoB) and the Arabian Sea (AS) in the left panel. Black-filled circles in the right panel denote the location of observation sites used in the model evaluation.

While understanding the characteristics and implications of BC particles has been a forefront area of research globally, it has special significance in developing regions of the world such as South Asia, where BC emissions and associated radiative perturbation are significantly higher than the globally averaged estimates [*Ramanathan and Carmichael*, 2008]. Model results suggest that strong BC emissions in South Asia have the potential to affect the major freshwater resources in this region, i.e., the Indian summer monsoon [e.g., *Ramanathan et al*., 2005; *Lau et al*., 2006; *Lau and Kim*, 2010] and Himalayan glaciers [e.g., *Menon et al*., 2010; *Yasunari et al*., 2010]. The research on BC in South Asia, particularly in India, started nearly two decades ago with the "Indian Ocean Experiment (INDOEX)," which revealed the presence of significant amounts of BC over the tropical Indian Ocean and highlighted the impacts BC can have on the regional climate and hydrology [*Lelieveld et al*., 2001; *Ramanathan et al*., 2001]. Soon after INDOEX, first measurements of BC with a complete seasonal cycle were reported from a tropical coastal site (Trivandrum) in India by *Babu and Moorthy* [2002]. The number of BC measurement stations has grown rapidly since then, and year-round BC observations have been available for more than 20 locations in India (see Figure 1).

BC measurements over India show that near surface BC mass concentrations exhibit a well-defined seasonal cycle with the highest values during winter and lowest during the monsoon season. This seasonal cycle is attributed to variations in the regional meteorology as well as the emissions of BC from a variety of anthropogenic and biomass burning sources. However, the relative contributions of these processes to the BC seasonality have not yet been quantified, and this forms the main objective of this study. The second objective of this study is to establish the seasonality of source-receptor relationships and transport pathways of black carbon (BC) aerosols in India.

We use the Weather Research and Forecasting Model [*Skamarock et al*., 2008] coupled with Chemistry (WRF-Chem) [*Grell et al*., 2005] to address the above stated two objectives by applying an explicit emission tagging technique [*Kumar et al*., 2015]. Previous regional and global modeling studies have also attempted to simulate the BC seasonal cycle over the Indian region, but significant deviation (by a factor of 2 to 5) of model results from the measurements inhibited such an analysis [e.g., *Nair et al*., 2012; *Moorthy et al*., 2013]. *Adhikary et al*. [2007] successfully reproduced the observed BC mass concentration at Hanimaadhoo climate observatory but could not capture the observed BC seasonal cycle at Kathmandu due to lack of brick kiln emissions within Kathmandu valley in their emission inventory. *Henriksson et al*. [2011] studied the seasonal cycle of aerosols in India and showed that their model qualitatively captures the differences in spatial patterns of sulfate and carbonaceous aerosols, and spatial distribution of aerosol optical depth, but they did not evaluate modeled BC quantitatively. The discrepancies between observations and models in these studies were mainly attributed to errors in boundary layer mixing/parameterization, uncertainties in BC

emissions estimates, and coarse spatial resolution of the models [e.g., *Nair et al*., 2012; *Moorthy et al*., 2013; *Michael et al*., 2014; *Joshi et al*., 2014]. However, the knowledge of BC emissions since then has advanced with recent developments of high resolution anthropogenic (0.1°) [*Janssens-Maenhout et al*., 2015; *Sadavarte and Venkataraman*, 2014; *Pandey et al*., 2014] and biomass burning (1 km) [*Wiedinmyer et al*., 2011] emission inventories. Additionally, the increase in computational ability has allowed us to use models at much finer resolution. In this study, we take advantage of these recent developments and conduct a year-long high resolution (10 km) simulation for the Indian region.

The paper is organized as follows. We begin with a description of the experimental design followed by the evaluation of the WRF-Chem simulated seasonal cycle with observations reported for the Indian region. We then quantify the contribution of different processes that control the seasonal cycle of BC over the Indian region and show how transport of BC changes with seasonal variations in meteorology. Finally, we summarize our main findings.

2. Experimental Design

2.1. The Observational Database

In this study, we use monthly average BC mass concentrations reported from 21 South Asian surface sites, listed in Table 1. These sites cover nearly the entire spatial extent of India (Figure 1) and represent a wide range of environments ranging from urban (Delhi, Kanpur, Bangalore, Ahmedabad, Hyderabad, and Kharagpur), semi-urban (Pantnagar and Nagpur), rural (Naliya, Dibrugarh, Anantapur, and Agartala), coastal (Trivandrum and Bhubaneswar), island (Port-Blair and Minicoy), to high altitude (Nainital, Hanle, Ooty, and NCO-P). BC measurements at all of these sites are made using multi-wavelength Aethalometers (Magee Scientific, USA), which deploy a filter-based optical attenuation technique assuming a mass-specific absorption cross section of 16.6 m^2 g^{-1} at 880 nm [*Hansen et al*., 1984]. The filter-based optical attenuation technique suffers from inherent uncertainties associated with shadowing and multiple scattering effects, and these uncertainties are estimated to contribute up to ~20% uncertainty in the measurements [*Arnott et al*., 2005; *Nair et al*., 2008]. Another source of uncertainty in Aethalometer measured mass concentration could be due to variations in the assumed BC mass-specific absorption cross section [*Nair et al*., 2012].

We also obtain the planetary boundary layer height (PBLH) derived for 31 sites (Table 1) within the model domain from the Integrated Global Radiosonde Archive (IGRA) [*Durre et al*., 2006; *Durre and Yin*, 2008] (available at http://www.ncdc.noaa.gov/oa/climate/igra/). The radiosonde observations, which form the basis of this derived PBLH data set, are carried out by the Indian Meteorological Department. The uncertainty in these PBLH estimates is estimated to be around a few 100 m [*Seidel et al*., 2010]. Radiosonde observations are also available at some other sites in the domain, but those are not used here because of the limited number of samples (less than 50 samples per year) available during 2011. In addition, we use the monthly accumulated precipitation product (3B42 algorithm) from the Tropical Rainfall Monitoring Mission (TRMM) for evaluating WRF-Chem. This precipitation product is available at a spatial resolution of $0.25° \times 0.25°$ and has been shown to accurately capture the climatology and rainfall variability over India [*Nair et al*., 2009]. This product has also been used previously for evaluation of WRF simulated rainfall over the Indian region [*Rakesh et al*., 2009; *Kumar et al*., 2012a].

2.2. The WRF-Chem Description

We use version 3.5.1 of the WRF-Chem model to simulate the distribution of BC over the South Asian region. In recent work, we have demonstrated the ability of WRF-Chem to capture important features of variations in meteorology and the distribution of selected trace gases [*Kumar et al*., 2012a, 2012b, 2013, 2014b; *Ghude et al*., 2013, 2014; *Jena et al*., 2014] and aerosols including BC [*Kumar et al*., 2014a, 2015] over the Indian region. However, the model's ability to simulate the complete seasonal cycle of BC has not yet been tested. In this study, the model domain covers the South Asian region with a horizontal grid spacing of 10 km (Figure 1) and 36 levels from the surface to 10 hPa. The horizontal grid spacing is limited by the resolution of anthropogenic emissions which are provided at 0.1° resolution.

Cloud microphysics is represented by the Thompson double moment microphysics [*Thompson et al*., 2008], and subgrid convection is represented by the Grell-3D scheme [*Grell and Devenyi*, 2002]. The Yonsei University

Table 1. List of Sites, Where BC and PBLH Observations are Available for Model Evaluation of BC Mass Concentration and PBLH[a]

S. N.	Site Name	Lon (°E)	Lat (°N)	Data	Data Source
1	Delhi	77.18	28.58	BC and PBLH	*Tiwari et al.* [2013], IGRA
2	Kanpur	80.32	26.46	BC	*Kanawade et al.* [2014]
3	Pantnagar	79.50	29.00	BC	*Joshi et al.* [2014]
4	Dibrugarh	94.60	27.30	BC and PBLH	*Pathak et al.* [2010], IGRA
5	Ahmedabad	72.60	23.03	BC and PBLH	*Ramachandran and Kedia* [2010], IGRA
6	Nagpur	79.15	21.15	BC and PBLH	*Kompalli et al.* [2014], IGRA
7	Bhubaneswar	85.25	21.25	BC and PBLH	*Mahapatra et al.* [2014], IGRA
8	Pune	73.85	18.53	BC	*Safai et al.* [2013]
9	Hyderabad	78.40	17.48	BC and PBLH	*Dumka et al.* [2013], IGRA
10	Kharagpur	87.32	22.33	BC	*Nair et al.* [2012]
11	Trivandrum	76.90	08.60	BC and PBLH	*Moorthy and Babu* [2006], IGRA
12	Anantapur	77.65	14.62	BC	*Reddy et al.* [2012]
13	Bangalore	77.59	12.97	BC	*Nair et al.* [2010]
14	Port-Blair	92.73	11.67	BC and PBLH	*Moorthy and Babu* [2006], IGRA
15	Minicoy	73.04	8.30	BC and PBLH	*Vinoj et al.* [2008], IGRA
16	Naliya	68.89	22.23	BC	*Gogoi et al.* [2013]
17	NCO-P	86.82	27.95	BC	*Nair et al.* [2013]
18	Agartala	91.26	23.76	BC	*Guha et al.* [2015]
19	Nainital	79.45	29.36	BC	*Dumka et al.* [2010]
20	Hanle	78.96	32.78	BC	*Nair et al.* [2013]
21	Ooty	76.43	11.23	BC	*Udayasoorian et al.* [2014]
22	Srinagar	74.83	34.08	PBLH	IGRA
23	Jodhpur	73.02	26.30	PBLH	IGRA
24	Lucknow	80.88	26.75	PBLH	IGRA
25	Gorakhpur	83.37	26.75	PBLH	IGRA
26	Siliguri	88.37	26.67	PBLH	IGRA
27	Gauhati	91.58	26.10	PBLH	IGRA
28	Patna	85.10	25.60	PBLH	IGRA
29	Bhopal	77.35	23.28	PBLH	IGRA
30	Ranchi	85.32	23.32	PBLH	IGRA
31	Agartala	91.25	23.88	PBLH	IGRA
32	Calcutta	88.45	22.65	PBLH	IGRA
33	Raipur	81.65	21.23	PBLH	IGRA
34	Mumbai	72.85	19.12	PBLH	IGRA
35	Aurangabad	75.40	19.80	PBLH	IGRA
36	Jagdalpur	82.03	19.08	PBLH	IGRA
37	Visakhapatnam	83.30	17.72	PBLH	IGRA
38	Machilipatnam	81.13	16.18	PBLH	IGRA
39	Panjim	73.82	15.48	PBLH	IGRA
40	Chennai	80.18	13.00	PBLH	IGRA
41	Panambur	74.83	12.95	PBLH	IGRA
42	Karaikal	79.83	10.92	PBLH	IGRA
43	Cochin	76.23	09.93	PBLH	IGRA

[a]Data column shows whether a site has both BC and PBLH data available or only one of the two. Data source is given in the rightmost column.

Scheme [*Hong et al.*, 2006] is employed as the planetary boundary layer scheme, and the Noah land surface model [*Tewari et al.*, 2004] is used to provide heat and moisture fluxes over land. The short-wave radiation is represented by the Goddard short-wave scheme [*Chou and Suarez*, 1994], while long-wave radiation is represented by the Rapid Radiative Transfer Model [*Mlawer et al.*, 1997].

We use the Goddard Chemistry Aerosol Radiation and Transport (GOCART) bulk aerosol scheme [*Chin et al.*, 2000, 2002] to represent aerosol processes in the model. This scheme does not simulate ozone chemistry, but we chose this scheme because it is computationally efficient and able to address the objectives of this study. The GOCART scheme simulates five major tropospheric aerosol types including black carbon, organic carbon, sulfate, dust, and sea salt, assuming externally mixed aerosols. BC aerosols in GOCART are considered to be present in hydrophobic and hydrophilic modes with a hydrophobic-to-hydrophilic conversion e-folding lifetime of 2.5 days. All primary BC emissions are assumed to occur in hydrophobic mode. BC is removed

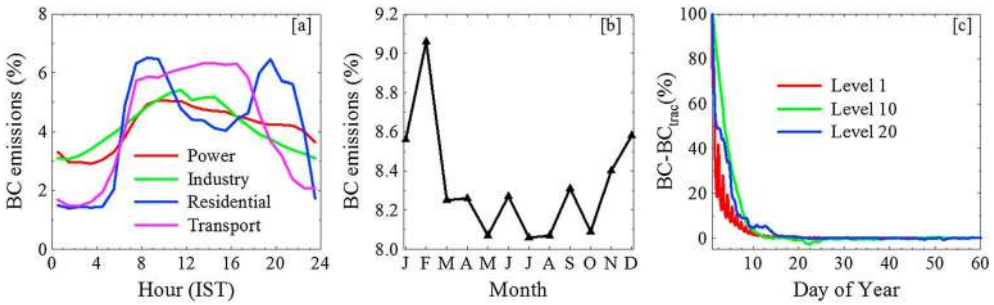

Figure 2. (a) Diurnal and (b) seasonal variations of anthropogenic emissions used in this study. (c) Time series of percentage difference between total simulated BC and sum of all the BC tracers (BCtrac = BC-ANT + BC-BB + BC-BDY) at the first, 10th, and 20th model levels. The fractions on the *y* axis in Figure 2a represent relative contribution of each hour to the total daily emissions, while those in Figure 2b represent relative contribution to annual total emissions.

by dry deposition from both the hydrophobic and hydrophilic modes and by wet deposition from the hydrophilic mode. The dry deposition of aerosols is computed using a series resistance approach [*Walcek et al*., 1986; *Wesely*, 1989], which assumes that deposition velocity of aerosols is inversely proportional to the sum of three resistances called aerodynamic resistance, sublayer resistance, and surface (canopy) resistance. These resistances are parameterized in terms of the friction velocity, Monin-Obukhov length scale, and the planetary boundary layer height following the equations given in *Walcek et al*. [1986]. The hydrophilic BC is subjected to in-cloud scavenging in both the resolved and nonresolved scale precipitation by assuming that 80% of the hydrophilic BC can be incorporated in the cloud droplets. The lack of impaction scavenging in the model may lead to errors in the simulated BC distribution especially during the summer monsoon season, but it is difficult to quantify these errors at this stage due to lack of relevant observations.

Anthropogenic emissions of BC and other trace species are taken from the Emission Database for Global Atmospheric Research developed for the assessment of Hemispheric Transport of Air Pollutants (EDGAR-HTAP; http://edgar.jrc.ec.europa.eu/htap_v2/index.php?SECURE=123). This database provides monthly varying global anthropogenic emissions at a spatial resolution of $0.1° \times 0.1°$ for the year 2010 and is based on a combination of nationally reported emissions and region-specific inventories. The seasonal cycle is based on monthly activity data for transportation, power generation, and industrial sectors, and on dependence of cooking stove operations on regional monthly mean temperature for residential sector [*Lu et al*., 2011].

We introduced a diurnal cycle in the anthropogenic BC emissions following *Olivier et al*. [2003]. This diurnal variation is based primarily on data from Western Europe and thus does not necessarily represent the diurnal variation in anthropogenic activities over India. However, this represents the current state of knowledge and is useful to assess the sensitivity of simulated BC to diurnal variation in anthropogenic emissions until a comprehensive compilation and assessment of actual variations becomes available. The diurnal and seasonal variations in anthropogenic BC emissions used here are shown in Figures 2a and 2b, respectively. On a diurnal scale, anthropogenic emissions of BC from all the sectors are higher during daytime and lower during nighttime. BC emissions from the residential sector show two distinct peaks in the morning and evening, while those from other sectors show a broader daytime maximum of varying duration. The seasonal cycle in BC emissions is characterized by higher values in the winter (December–February) and lower values during monsoon season (June–September).

Daily varying biomass burning emissions of BC and other aerosol species are obtained from the Fire Inventory from NCAR [*Wiedinmyer et al*., 2011] and are distributed vertically in the model following the online plume-rise module [*Freitas et al*., 2007]. The spatial distributions of annual average anthropogenic and biomass burning emissions are shown in Figure 1. The highest anthropogenic BC emissions occur along the Indo-Gangetic Plain, while the highest biomass burning emissions are seen over Burma. Time series analysis of biomass burning emission shows that the highest biomass burning activity generally occurs during March–May.

Total anthropogenic and biomass burning emissions over the model domain for the year 2011 are estimated to be about 1354 Gg and 481 Gg, respectively. The annual total anthropogenic BC emission estimates are

slightly higher compared to other regional inventories such as System for Air quality Forecasting And Research-India (~1110 Gg), Regional Emission Inventory for Asia (~1170 Gg), and Southeast Asia Composition, Clouds and Climate Coupling by Regional Study (~1195 Gg), but are significantly higher compared to the Intercontinental chemical Transport Experiment Phase B inventory (~550 Gg).

Initial and lateral boundary conditions for meteorological fields are obtained from European Center for Medium Range Weather Forecasts atmospheric operational model analyses and products available every 6 h at a fine horizontal grid spacing of 0.141°. Initial and boundary conditions for BC and other aerosols are based on Model for Ozone and Related Tracers (MOZART-4) model output [*Emmons et al*., 2010].

We implemented 10 BC tracers on top of the standard BC particles in the WRF-Chem model to track BC emitted from different source types and regions and to understand the relative importance of emissions and meteorology in controlling the seasonal cycle of BC. BC tracers are artificial species added to the simulation that experience the same atmospheric processes (emission, transport, aging, dry, and wet deposition) like a standard BC particle. However, the tracers do not affect the standard model results. We account for all sources of BC in the model by tracking BC emitted from anthropogenic (BC-ANT) and biomass burning (BC-BB) sources within the domain, and BC inflow from the lateral domain boundaries (BC-BDY). The BC-BDY tracer includes the contribution from all BC emission sources located outside the selected domain, and therefore, its distribution will provide information about background BC levels for South Asia.

Four regional tracers track BC emitted from sources in North, West, East, and South India, respectively (Figure 1a). Anthropogenic emissions of BC from outside these five regions are also tracked separately and are classified as "other regions." The initial and boundary conditions for all BC tracers are set to zero except boundary conditions for BC-BDY, which are set equal to BC from MOZART-4. Two additional tracers are defined as BC_NS and BC_ND to understand the sensitivity of simulated BC with respect to seasonal and diurnal variations of anthropogenic BC emissions. BC_NS and BC_ND are similar to standard BC except that anthropogenic emissions contributing to BC_NS and BC_ND do not have a seasonal and diurnal cycle, respectively. BC-NS, BC_ND, and the four regional tracers are introduced as an emission type in the model, while BC-ANT and BC-BB are determined from standard input anthropogenic and biomass burning emissions.

In this study, we do not tag BC by sector as we did in our previous study [*Kumar et al*., 2015] because we found that the contributions of residential, industrial, transport, and power generation emission sectors to total anthropogenic emissions and to the surface anthropogenic BC mass concentrations in North, West, East, and South India are nearly identical [*Kumar et al*., 2015], although there is transport of air masses between these regions. Therefore, we conclude that the contribution of different sectors to surface BC mass concentration can be inferred by analyzing the contribution of different sectors to total BC anthropogenic emissions, and we do not need separate tags for different sectors.

However, it should be noted that the nearly identical contribution of different sectors to BC emissions and surface mass concentrations found in *Kumar et al*. [2015] is a result of several factors: (1) BC is a primary pollutant, (2) BC is not affected by atmospheric chemistry, (3) the geographical regions (North, West, East, and South India) do not differ significantly in terms of the relative contribution of different sectors to total anthropogenic BC emissions, and (4) the loss processes do not change the percent contributions of different sectors during transport of BC from one region to the other. If any one of these conditions is not satisfied, then the contribution of different sectors to surface BC mass concentration cannot be inferred directly by analyzing the contribution of different sectors to total BC anthropogenic emissions, and it would become important to tag BC by sector to quantify the contribution of different sectors to surface BC mass concentration in different regions. Such a situation may arise, for example, if people living in North India start using a different fuel (e.g., LPG) for cooking, but people in East India continue using solid biofuels for cooking.

In addition to the BC tracers, four BC tendency terms including net vertical mixing, convective transport, and horizontal and vertical advection are monitored during the simulation. These tendency terms represent different terms contributing to the time rate change of BC in prognostic equation of BC. The horizontal and vertical advection tendency terms of BC are obtained from the fluxes calculated in the advection scheme that are multiplied by the area of the grid cell face and time step. The convective transport and vertical mixing tendency terms are found by differencing the mixing ratios of BC before and after each process. This concept of tendencies has been used before in WRF-Chem to understand processes

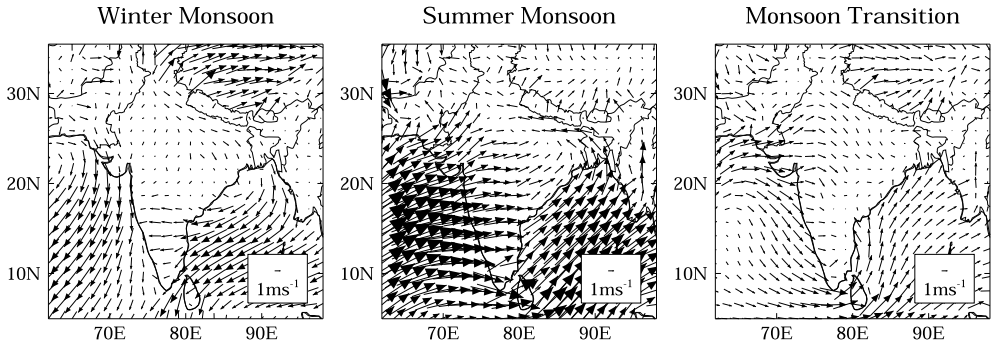

Figure 3. WRF-Chem simulated average wind vectors at 10 m during winter monsoon, summer monsoon, and monsoon transition seasons. Wind vectors are shown every 15th grid point for clarity.

controlling selected trace gases [e.g., *Barth et al*., 2012] but is being utilized for the first time for aerosols. We also keep track of the accumulated dry and wet deposition amounts of BC.

The model simulations started on 01 Jan 2011 at 0000 UTC with a time step of 60 s and ended on 31 Dec 2011 at 23 UTC. The model results are saved every hour for further analysis. The tracers are assumed to be well spun up when the sum of BC tracers (BC_{trac} = BC-ANT + BC-BB + BC-BDY) approaches the total simulated BC. The time series of the relative difference between domain-wide averaged BC and BC_{trac} (Figure 2c) at the first, 10th, and 20th model level shows that the difference rapidly approaches 0% in the first 15 days of the simulation and remains close to zero thereafter. Thus, all tracers are reasonably well spun up by 20 Jan 2011. For the standard model species including BC particles, a spin-up time of 48 h was used to minimize the effect of initial conditions. The choice of spin-up time for standard species is based on previous studies [e.g., *Jimenez et al*., 2005] and our past experience with WRF-Chem modeling.

2.3. Regional Meteorology of South Asia

In this section, we provide a brief description of the regional meteorology of South Asia because it plays an important role in controlling the seasonal cycle of BC over this region. The regional meteorology of South Asia is dominated by the Asian monsoonal circulation and can be broken down into three basic seasons: the winter monsoon (WM) season, summer monsoon (SM) season, and monsoon transition (MT) seasons. The exact timing of these seasons may vary each year, but WM generally occurs during November–March, SM during June–September, and MT season during April–May for winter-to-summer transition and during late September–October for summer-to-winter transition. In this study, we have defined WM season as 1 November to 31 March, SM season as 1 June to 30 September, and 1 April to 30 May and 1–31 October as MT season.

The WRF-Chem simulated average wind vectors at 10 m during these three defined seasons are shown in Figure 3. Average surface winds are weaker over land as compared to ocean for all seasons due to higher surface roughness over land. The WM season is characterized by offshore winds, which leads to dry atmospheric conditions and facilitates the transport of pollutants from land to ocean. In contrast, the SM season is characterized by onshore winds which bring moisture from ocean over land, causing large-scale rainfall leading to the washout of aerosols. The cleaner marine air masses associated with SM onshore winds can also potentially dilute pollutants over land. The meridional monsoonal winds weaken during the MT season, and the zonal transport becomes more important especially north of 20°N. The transport of pollutants from land to ocean is also limited during the MT season due to the prevalence of northerly winds over the Arabian Sea and southerly winds over the Bay of Bengal. Further details about the regional meteorology of South Asia can be seen elsewhere [*Asnani*, 2005; *Lawrence and Lelieveld*, 2010; *Kumar et al*., 2012a].

Since wet scavenging is an important removal process for BC, we evaluate the modeled precipitation by comparing the WRF-Chem predicted accumulated precipitation with the TRMM retrieved accumulated precipitation for the three defined seasons (Figure 4). WRF-Chem successfully captures the seasonal cycle of precipitation as seen by TRMM over most of the model domain. Both WRF-Chem and TRMM show an

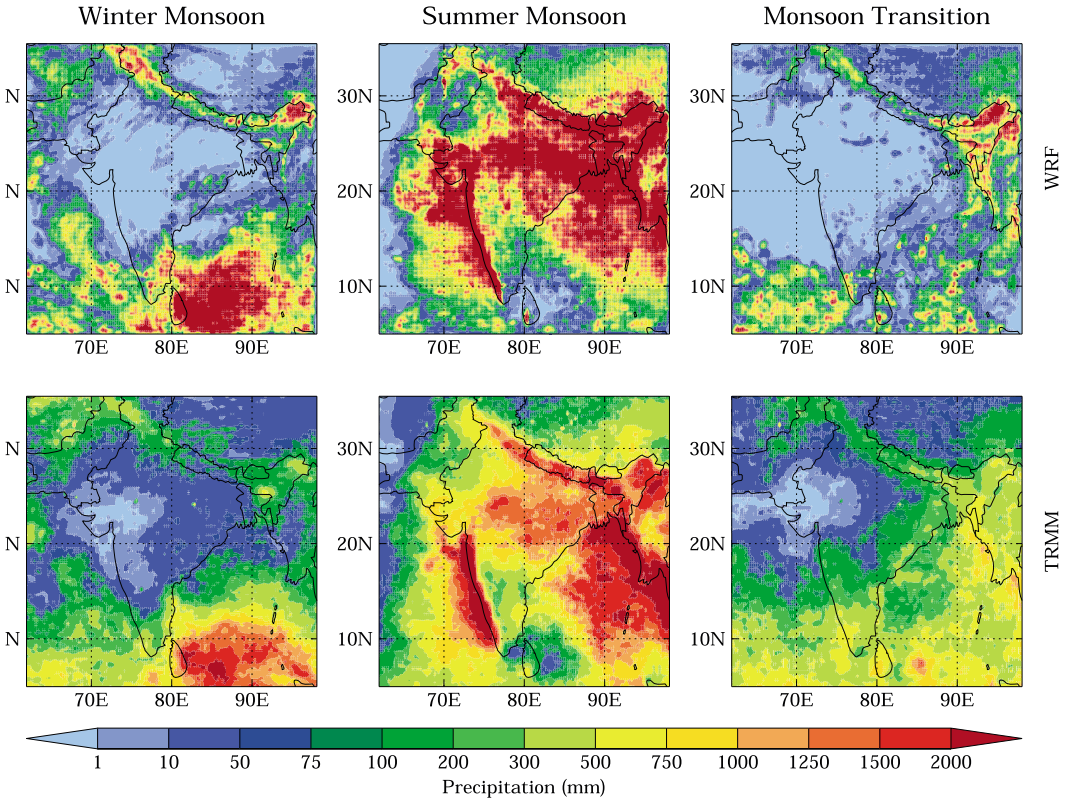

Figure 4. Comparison of (top) WRF-Chem simulated and (bottom) TRMM retrieved total precipitation during winter monsoon, summer monsoon, and monsoon transition seasons. For this comparison, a WRF-Chem value is derived for each TRMM grid box by adding all WRF-Chem values falling in that grid box.

increase in precipitation from WM season to SM season and a decrease from SM season to MT season, but there are some differences in the spatial distribution as well as absolute magnitude. In general, the model overestimates the precipitation seen by TRMM during all seasons except during MT season when the model shows an underestimation over several parts of the domain including Arabian Sea, southern India, the Bay of Bengal, the Indo-Gangetic Plain, and the Himalayan foothills. Analysis of the modeled precipitation shows that about 60% of the rainfall in the model results from the convective parameterization. Note that accurate simulation of monsoonal rainfall over South Asia has been a challenging task and limited ability of regional models (MM5 and WRF) in this regard has also been reported in previous studies [e.g., *Ratnam and Kumar*, 2005; *Rakesh et al.*, 2009; *Kumar et al.*, 2012a]. However, *Kumar et al.* [2012a] showed that the probability of detecting a rainfall event is greater than the false simulation of a rainfall event in WRF. *Kumar et al.* [2012a] also conducted a detailed evaluation of other meteorological parameters (temperature, winds, water vapor, dew point temperature, and tropopause pressure) over this domain and concluded that WRF simulated meteorology is of sufficient quality for use in air quality simulations.

3. Results and Discussion

3.1. Model Evaluation

We first evaluate the performance of WRF-Chem in simulating the seasonal cycle of BC over the Indian region by comparing model simulated surface layer BC mass concentrations with observed values reported in the literature at 21 sites in the Indian region (Figure 5). The observed BC mass concentrations show the highest values during the WM season at all the sites except at Bangalore, Nainital, NCO-P, and Hanle, where the highest values are seen during the MT season (April–May). Lowest BC mass concentrations at all the sites are observed during the SM season. The model reproduces the observed seasonal cycle in BC

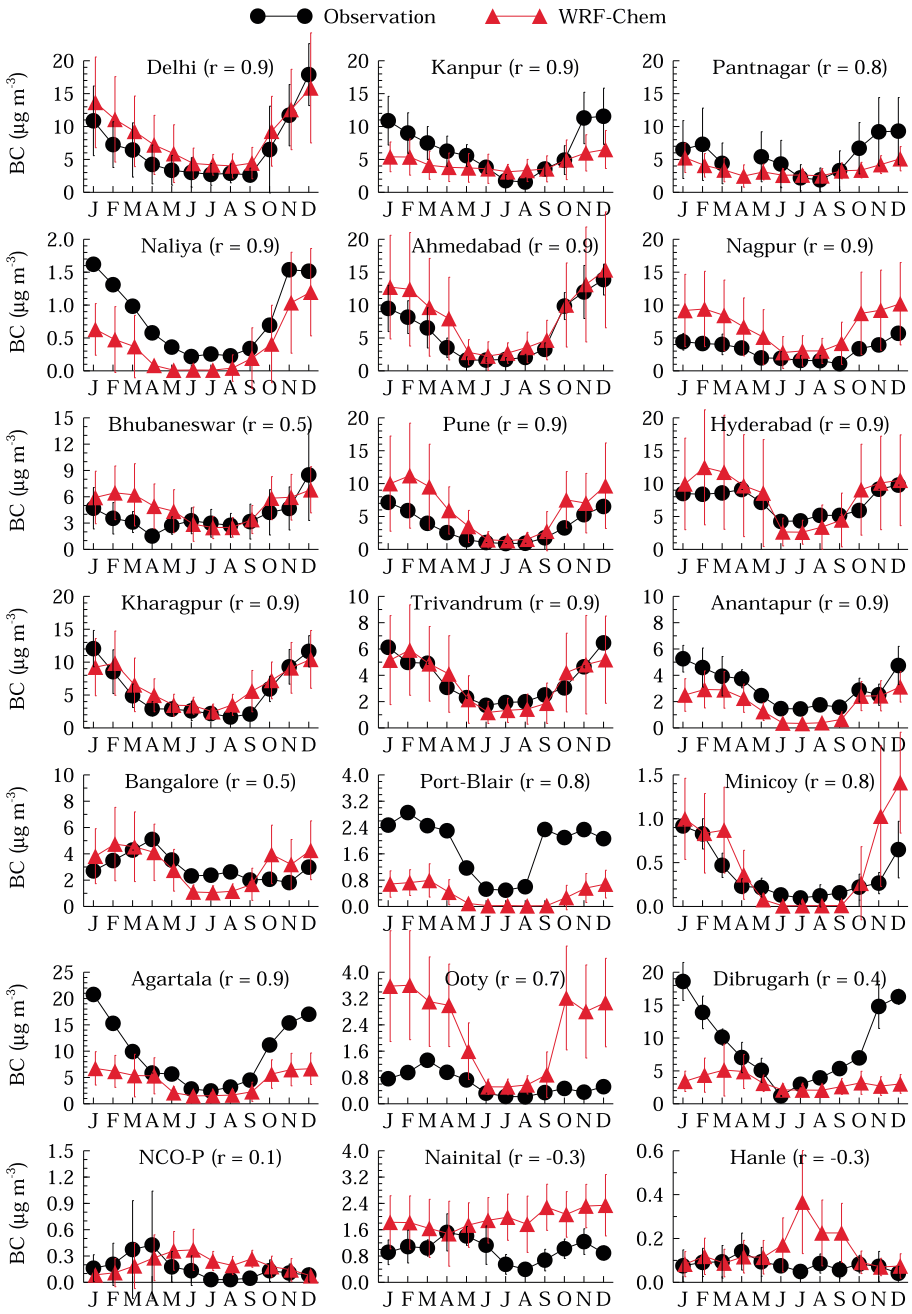

Figure 5. Comparison of observed and WRF-Chem simulated seasonal cycles of BC mass concentrations at 21 Indian sites. The vertical bars represent standard deviation in average values. Standard deviations in observations for some of the sites could not be retrieved from the literature and are not shown. The name of observation site and correlation coefficient between model and observation are also shown in each panel.

mass concentrations fairly well ($0.52 < r < 0.95$) at 17 of 21 sites considered here, and the magnitude of simulated BC at several sites is much closer to the observations compared to previous studies. For example, *Moorthy et al.* [2013] reported that the ratio of measured to modeled (GOCART and CHIMERE) BC mass concentration at Delhi, Kharagpur, Trivandrum, Minicoy, Port-Blair, and Nainital ranged from 0.7 to 6, while the corresponding ratios in our study range from 0.2 to 1.5. Further, *Nair et al.* [2012] reported a ratio of about 10 for Hyderabad in the RegCM4 model, while the corresponding ratio in our simulations ranges from 0.6 to 1.7. The model fails to capture the seasonality at four of the sites (Dibrugarh, Nainital, NCO-P, and Hanle). In addition, differences in the absolute magnitude of BC between the model and observations

are discerned at several sites, where ratio of measured to simulated BC mass concentration exceeds 2 especially for the nonsummer months. Possible reasons for discrepancy between the modeled and observed BC mass concentration are discussed below.

Dibrugarh in northeast India is a rural site surrounded by tea gardens, rivers, and other water bodies, but BC mass concentrations at this site are comparable to or even higher than those observed at urban sites (Delhi, Bangalore, Hyderabad, Kanpur, Pune, Ahmedabad, etc.) in India due to presence of many oil refineries near the measurement site (50–100 km) [*Pathak et al.*, 2010]. Large differences between modeled and observed BC mass concentration point toward underestimation of anthropogenic BC emissions from these oil refineries. The peak in modeled BC at Dibrugarh during March–April is due to additional contribution from biomass burning emissions.

Nainital, NCO-P, and Hanle are located in the Himalayan region and represent cleaner high altitude environments. We also compared model predicted seasonal cycle of BC with two urban valley sites, namely, Dehradun [*Kant et al.*, 2012] and Kullu [*Sharma et al.*, 2013] located in the Himalayan region (not shown), and the model failed to capture the observed seasonal cycle of BC at these sites. The discrepancy at these Himalayan sites could be associated with uncertainties in BC emissions along with errors in representation of topography around these sites in the model and associated errors in the meteorological processes. Local emissions should have minimal impact at Nainital and Hanle as these sites are located reasonably far from major BC emission sources [*Dumka et al.*, 2010; *Nair et al.*, 2013]. The altitudes of Hanle and Dehradun is represented reasonably well by the model with differences of less than 50 m, but the model has put Kullu at a higher elevation (2080 m compared to 1155 m) and Nainital at a lower elevation (1350 m compared to 1958 m). Note that the width (0.5–2 km) of the Kullu valley is much smaller than the model grid spacing (10 km). The elevation of NCO-P is higher by about 500 m in the model. The elevation of Ooty, a high altitude site in southern India, is also lower by about 600 m in the model.

We analyzed BC source tracers at all the sites to identify the most important BC sources and found that BC mass concentrations at most of the sites are controlled by anthropogenic sources. This suggests that uncertainties in anthropogenic emission estimates likely make an important contribution to the discrepancies between model results and observations. We also examined the contribution of the diurnal cycle of anthropogenic emissions to the differences between the model and observations by comparing the diurnal variations of model simulated and observed BC mass concentrations at five sites (Delhi, Kanpur, Bhubaneswar, Pune, and Anantapur; Figure 6). Diurnal variation of BC_ND is also shown to depict the sensitivity of simulated BC mass concentration to diurnal variations in anthropogenic emissions. Note that this comparison is presented for four seasons instead of three defined earlier because diurnal variations in the literature have been reported for four seasons [*Tiwari et al.*, 2013; *Kanawade et al.*, 2014; *Mahapatra et al.*, 2014; *Safai et al.*, 2013; *Reddy et al.*, 2012]. It is seen that differences between the model and observations are largest during nighttime. In fact, daytime modeled and observed BC mass concentrations show fairly good agreement during all the seasons at Delhi, Bhubaneswar, and Pune and during monsoon seasons at Kanpur and postmonsoon at Anantapur. A comparison of WRF predicted BC and BC_ND shows that introducing a diurnal cycle in anthropogenic emissions of BC does not lead to a great improvement in the diurnal concentration profile but reduces the absolute differences between model and observations especially at Delhi and Pune. These model results indicate that comprehensive research effort is required not only in improving the total amount of BC emitted in this region but also in constructing the diurnal variability of anthropogenic emissions.

Larger differences in nighttime BC mass concentration between the model and observations might also be related to uncertainties in the estimation of PBLH by the model. We made an attempt to evaluate the model simulated PBLH through comparison with PBLH derived from radiosonde observations (Figure 7) at 00 UTC. For this we compared annual averages because the number of available observations (51–136) is not sufficient to produce reasonable statistics for individual seasons. Average observed and model simulated PBLH at 00 UTC are 100–650 m and 50–500 m, respectively. The model underestimates the observed PBLH by 20–450 m at all inland stations except at few coastal sites where the model shows an overestimation by 20–200 m. A shallow PBL in the model during nighttime will trap the pollutants in a smaller volume and lead to a model simulated concentration that is higher than the observations. However, more observations of PBLH covering the entire diurnal cycle are required to fully understand the role of boundary layer evolution in the model-observation discrepancy.

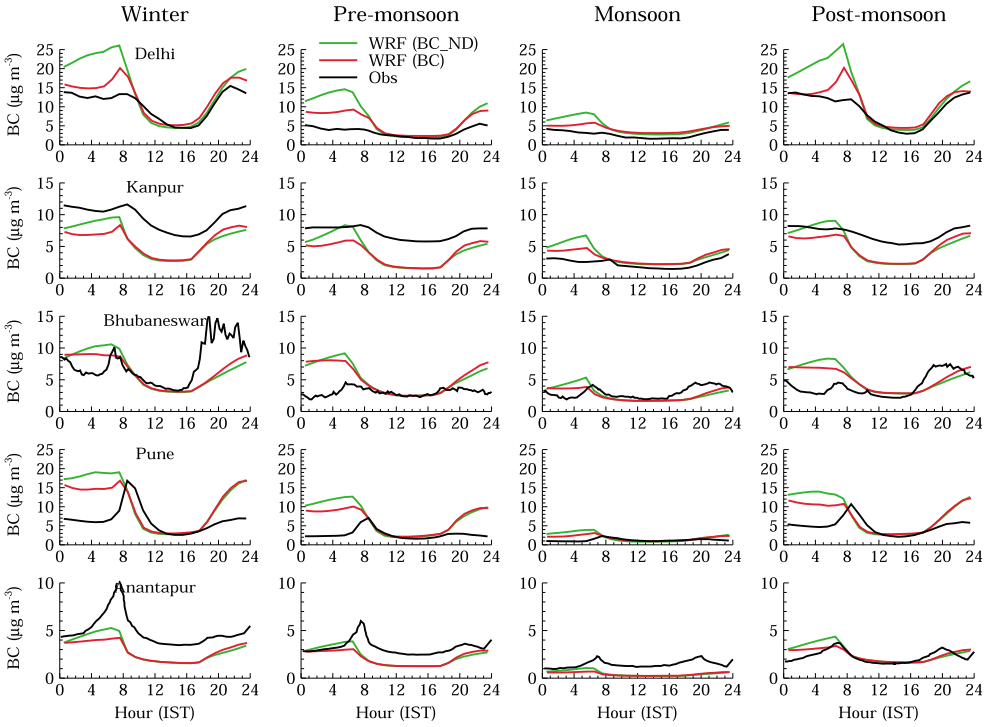

Figure 6. Comparison of observed and WRF-Chem simulated diurnal variation of BC mass concentrations at five Indian sites during winter, premonsoon, monsoon, and postmonsoon. Indian standard time (IST) is 5.5 h ahead of UTC. The black line represents the observed BC, while the red and green lines represent WRF-Chem simulated BC with and without including diurnal variations of anthropogenic emissions, respectively.

Apart from uncertainties in anthropogenic and biomass burning emissions, and PBLH estimates, the inflow of BC from the domain boundaries also contributes to model-observation discrepancy especially at Port-Blair where it contributes about 50 ± 34% to the modeled BC mass concentrations. Another important factor contributing to model-observation discrepancy could be uncertainty in the wet removal of BC in the model. The overestimation of monsoonal rainfall by the model may enhance the wet removal of BC in the model, while a slower aging of BC from the hydrophobic mode to the hydrophilic mode with an e-folding lifetime of 2.5 days and lack of impaction scavenging in the model might slow down the wet removal of BC [e.g., *Barth and Church*, 1999; *Wang et al*., 2014]. To examine the sensitivity of BC to the aging time and impaction scavenging, we conducted three sensitivity simulations.

In the first simulation, we reduced hydrophobic-to-hydrophilic conversion time of BC from 2.5 to 1.2 days. In the second simulation, we tested the sensitivity of the simulated BC distribution to impaction scavenging by introducing a very simple parameterization of impaction scavenging by assuming that 10% of the aerosol mass is removed by large-scale precipitation falling through the noncloudy model layers located below the cloud. In the third simulation, we used the detailed aerosol model called "Model for Simulating Aerosol Interactions and Chemistry (MOSAIC)" [*Zaveri et al*., 2008] to simulate BC distribution. MOSAIC treats BC as internally mixed with all other aerosol components and includes both in-cloud and impaction scavenging. The internal mixing assumption implies that there is no aging time from emissions of hydrophobic to hydrophilic BC. Note that MOSAIC is computationally much more expensive than GOCART and was run at 20 km resolution. For the same reason, the sensitivity simulations were conducted for only 1 month.

The time series of daily average BC mass concentration from these three sensitivity runs along with base run (presented in the manuscript) are compared to observations at Nainital (Figure S2 of the supporting information). All the model runs capture the observed decrease in BC mass concentration with time. The reduction of aging time from 2.5 to 1.2 days (GOCART_test_aging) does not make much difference compared to the base run (GOCART_base). However, inclusion of impaction scavenging (GOCART_test_wetdep) does reduce BC mass concentrations relative to the base case, but we are still too far from the observed values. MOZART-MOSAIC

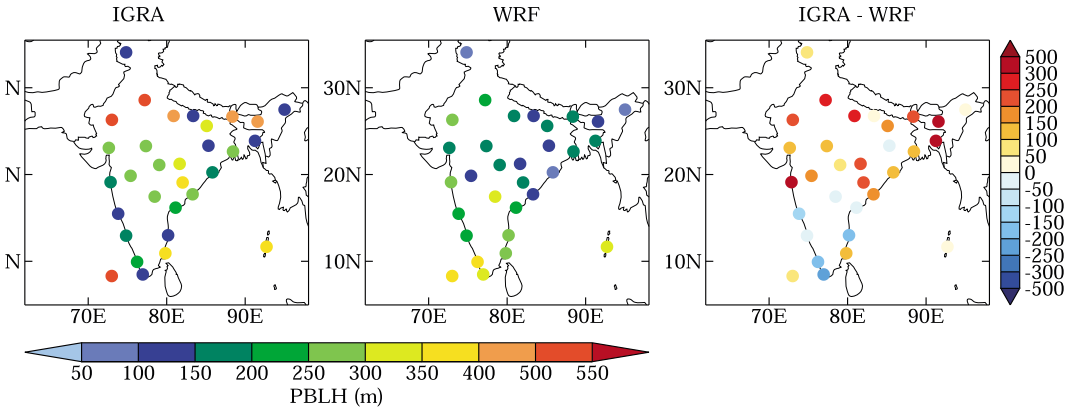

Figure 7. Comparison of observed (IGRA) and WRF-Chem simulated annually averaged PBLH at 00 UTC for 31 sites in the domain. Mean bias in the model simulated PBLH is also shown in the rightmost panel.

simulations show a stronger decrease, but we are still far from the observations. These results show that BC simulations are sensitive to parameterization of aging and removal efficiency, but we do not have enough observations to constrain these parameterizations.

To demonstrate our limited understanding of these processes, we compare the parameterization of these processes in WRF-Chem with those in GEOS-Chem [*Liu et al.*, 2011 and *He et al.*, 2014]. Both WRF-Chem and GEOS-Chem consider BC aerosols to be present in both hydrophobic and hydrophilic mode, but BC aging treatments in the two models are very different. WRF-Chem assumes all the primary BC emissions to occur in the hydrophobic mode, while GEOS-Chem assumes 80% of the primary BC emissions in the hydrophobic mode and 20% in the hydrophilic mode. The e-folding lifetime for hydrophobic-to-hydrophilic conversion is set as a constant value of 1 day in GEOS-Chem and 2.5 days in WRF-Chem, while a recent modeling study has shown that this time scale varies between day and night and can be between 0.068–11 h during daytime and 6.4–54 h during nighttime for an urban plume [*Riemer et al.*, 2010]. Since the hydrophobic-to-hydrophilic conversion determines the amount of aerosol mass incorporated into the cloud droplets, the errors in the aging parameterization lead to errors in the wet removal of aerosols on top of other errors introduced by wet removal parameterization itself. Similar to BC aging treatment, the wet scavenging treatment also differs between WRF-Chem and GEOS-Chem. WRF-Chem assumes that 80% of the hydrophilic BC partitions into cloud water, while GEOS-Chem assumes 100% incorporation of hydrophilic BC in the cloud water. In addition, complex topography of the Himalayan region makes it difficult to capture mesoscale transport processes, especially the mountain valley winds, which have been found to play a major role in controlling diurnal variability of trace species at these sites [e.g., *Dumka et al.*, 2010; *Nair et al.*, 2013].

In theory, we could perform a large number of sensitivity experiments to determine the best set of model parameters which can reduce the discrepancies between the model results and observations. But we do not want to follow this approach because such parameters will not have a strong scientific basis. We would prefer to wait for some relevant observations such as those of refractory BC mass, mixing state, and vertical distribution of BC aerosols to improve parameterization of these processes in the model.

The above discussion showed that discrepancy between the model and observations can be related to a number of factors including uncertainties in anthropogenic and biomass burning emission estimates, errors in model representation of landscape around high altitude sites, errors in model predicted meteorology, aerosol processes, numerical model error, and uncertainty in boundary conditions of BC mass concentrations provided from the global model. At this stage, it is not possible to validate model simulated vertical distribution of BC, but we have some confidence in the model's ability of simulating seasonal changes in the vertical transport based on our previous studies [*Kumar et al.*, 2012a, 2012b, 2014a]. In those studies, we have compared WRF-Chem simulated vertical distribution of ozone, carbon monoxide, water vapor, and dust plumes with available in situ and satellite based measurements. We have also shown that WRF-Chem also reproduces the spatial distribution of BC observed over the Bay of Bengal and the Arabian Sea [*Kumar et al.*, 2015]. While there are weaknesses in the model performance especially in representing the magnitude of observed BC and capturing BC seasonality in Himalayas, the ability of the

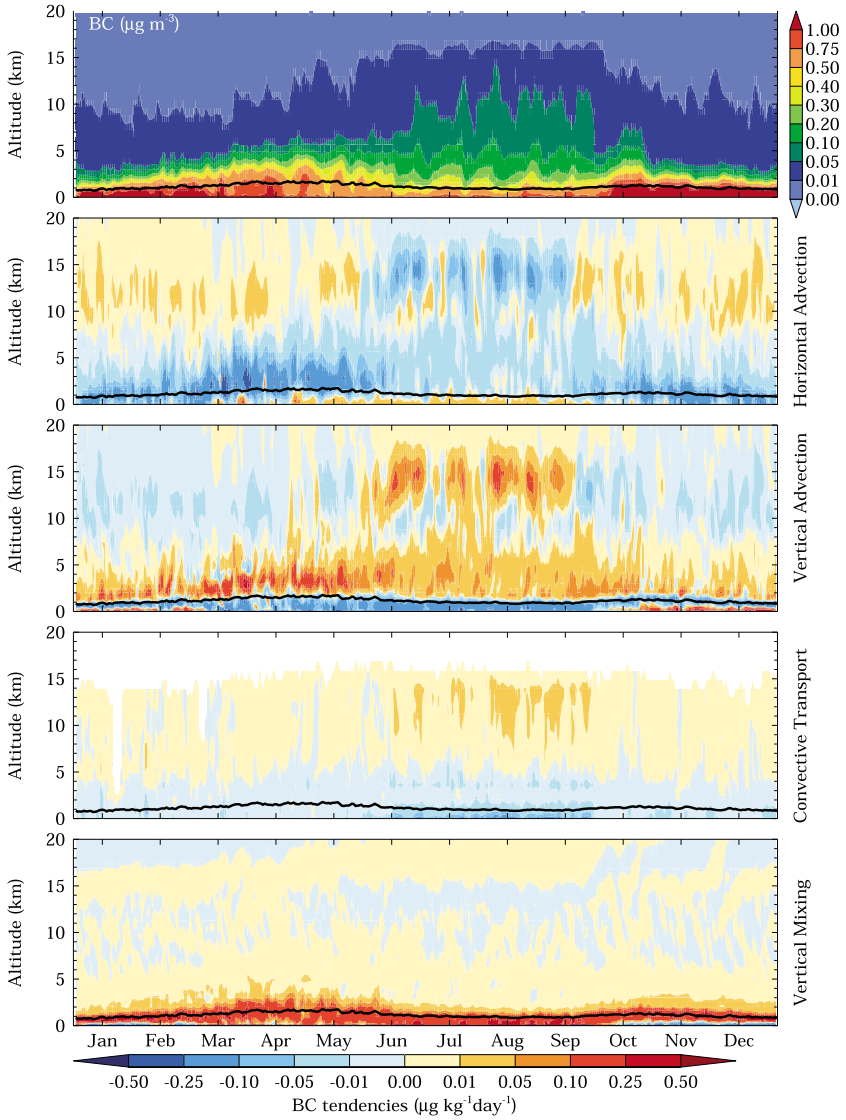

Figure 8. Vertical distribution of the daily averaged BC mass concentration and the daily accumulated BC tendencies due to horizontal and vertical advection, convective transport, and vertical mixing over the Indian region (68°–91°E, 7°–35°N). The solid and dotted black lines represent daily averaged PBL and thermal tropopause heights over the Indian region, respectively. White space indicates zero value of a tendency term.

model in capturing the observed seasonal cycle over most of the model domain provides confidence in using the model to understand processes controlling the seasonality of BC mass concentrations over the Indian region.

3.2. Processes Controlling the Seasonal Cycle of BC

To characterize the seasonal cycle of BC, we examined the vertical distribution of the daily averaged BC mass concentration over the Indian region (68°–91°E, 7°–35°N) (Figure 8). BC mass concentration in the lower troposphere (below 3 km) shows seasonal variation similar to the surface observations with the highest and the lowest values during the WM and SM seasons, respectively. In contrast, BC in the free troposphere (above 3 km) shows an opposite seasonal cycle with the highest and lowest values during the SM and WM seasons, respectively. The free tropospheric seasonal cycle of BC reported here is consistent with satellite retrievals of carbon monoxide [*Girach and Nair*, 2014] and peroxyacetyl nitrate [*Fadnavis et al.*, 2014], and global model simulation of aerosols including BC [*Fadnavis et al.*, 2013].

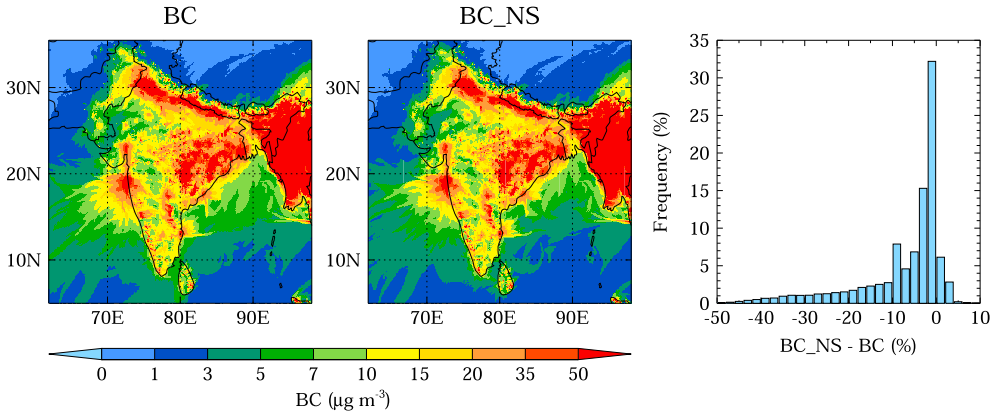

Figure 9. Spatial surface distributions of amplitude of seasonal cycle for BC and BC_NS for the year 2011. Frequency distribution of (BC_NS-BC) is also shown.

This seasonal cycle is driven by seasonal changes in regional BC emissions and meteorology. As BC emissions from anthropogenic sources (1354 Gg) are about three times higher than those from biomass burning (481 Gg) in our model domain, biomass burning emissions should not have a large influence on the seasonal cycle of BC over the larger Indian region (68°–91°E, 7°–35°N). However, biomass burning is very important over Burma where it accounts for about 80% of the total biomass burning occurring in our model domain.

To examine the influence of seasonal changes in anthropogenic emissions on the seasonal cycle of BC at the surface, we compare the spatial surface distributions of the seasonal amplitude of BC and BC_NS (Figure 9). The amplitude of the seasonal cycle for both BC and BC_NS is calculated by subtracting the annual minimum value from the annual maximum value in each grid box. The seasonal amplitude for both BC and BC_NS has similar magnitudes as well as spatial distributions, and most differences are less than 20% (rightmost panel, Figure 9). The average percentage difference between the amplitude of the seasonal cycle for BC and BC_NS is estimated as $6 \pm 10\%$, indicating that anthropogenic emissions do not control the seasonality of BC and therefore seasonal changes in meteorology must be the controlling factor.

To understand which meteorological processes are more important for the seasonal variability of BC over the Indian region, we analyze the vertical distribution of BC tendencies due to horizontal and vertical advection, convective transport, and vertical mixing (Figure 8, also see Figure S1 for details in the lowest 2 km). The BC tendency due to horizontal advection shows large seasonal variation below 1 km as this process mostly transports BC out of the Indian region during October–April (negative values) and brings BC into the Indian region during May–September (positive values). The horizontal advection generally transports BC out of the Indian region throughout the year between 1 and 8 km. Above 8 km, the horizontal transport brings BC into the Indian region during October–May and transports BC out of the Indian region during June–September. The vertical advection generally acts as a sink of BC in the PBL throughout the year except at a few levels between the surface and 0.5 km during October–March. Above the PBL, the vertical advection generally enhances BC in the lower to middle troposphere (up to 8 km) throughout the year. Above 8 km, the vertical advection generally acts as a source of BC during the summer monsoon season and as a sink during other times of the year. The convective transport lifts BC from the lower troposphere (surface to about 4 km) to the middle and upper troposphere, and this lifting, as expected, is the highest during the summer monsoon season. The vertical mixing always acts as a sink of BC at the surface and source of BC at higher altitudes.

The seasonal mean BC tendencies due to the horizontal and vertical advection, convective transport, and vertical mixing are estimated at the surface, and in the lower (0.1–3 km), middle (3–8 km), and upper troposphere (8–15 km), respectively, to examine the relative strength of these processes (Figure 10). At the surface, all the processes tend to remove BC except the horizontal advection during the SM season, but the distribution of BC is governed mainly by the vertical mixing as the magnitude of the vertical mixing term is 1–3 orders of magnitude higher compared to other processes. Note that the vertical mixing term includes contributions from both the dry deposition and vertical diffusion, and thus, we can estimate the

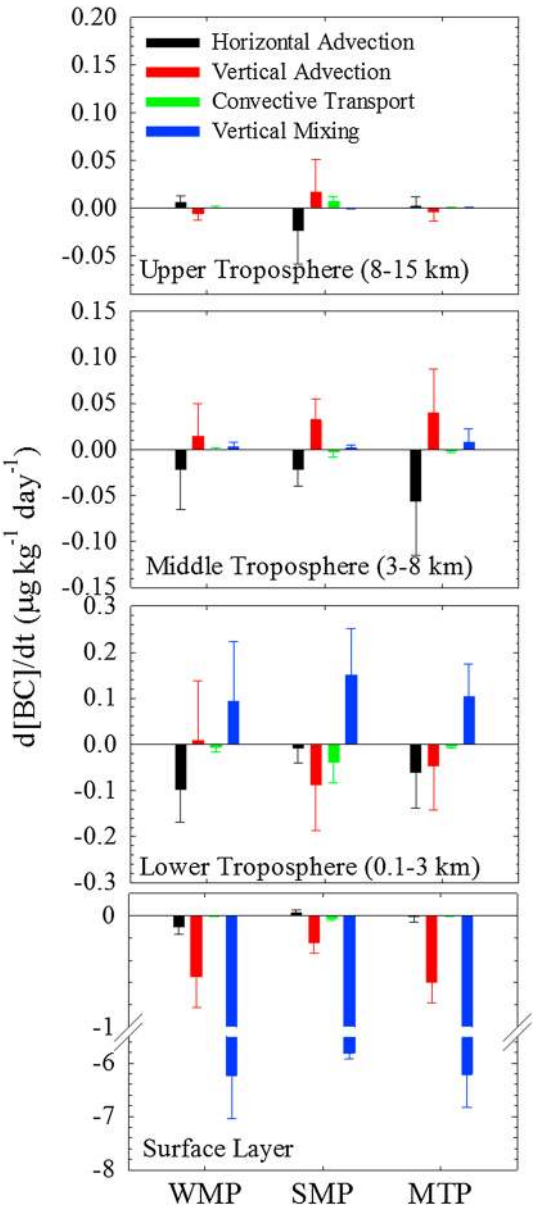

Figure 10. Seasonal mean BC tendency due to the horizontal and vertical advection, convective transport, and vertical mixing at the surface, and in the lower (0–3 km), middle (3–8 km), and upper (8–15 km) troposphere over the Indian region. The vertical bars show standard deviation and represent seasonal variability in mean tendency values.

relative contributions of these processes to the vertical mixing term at the surface by subtracting the dry deposited amount of BC from the surface layer vertical mixing term. The contributions of the dry deposition to the surface layer vertical mixing term during the WM, SM, and MT seasons over the Indian region are estimated as 38 ± 9%, 21 ± 2%, and 24 ± 6% respectively, while the corresponding contributions of the vertical diffusion term are estimated as 62 ± 9%, 79 ± 2%, and 76 ± 6%, respectively. These results suggests that the observed decrease in near surface BC mass concentrations from the WM to the SM season is driven mainly by an increase in the vertical diffusion of BC during the summer monsoon season.

The vertical mixing brings BC from the surface into the lower troposphere (0.1–3 km) throughout the year and is highest during the SM season. The direction (vertical or horizontal) in which BC is transported from the lower troposphere is determined by a competition between the horizontal and vertical advection. During the WM season, the effect of horizontal advection on BC is about 10 times stronger than the vertical advection, indicating that most of the BC from the lower troposphere is advected horizontally out of the Indian region and experiences very small vertical transport. This scenario reverses during the SM season when the effect of vertical advection on BC is about 10 times stronger than the horizontal advection and most of the BC undergoes vertical advection. The vertical transport of BC during the SM season is further enhanced by buoyant motions as the effect of convective transport on BC is also five times stronger than the horizontal advection. During MT season, BC is transported from the lower troposhere by both the horizontal and vertical advection. Note that a part of BC transported vertically is lost through wet deposition, which also shows a distinct seasonality with maximum in the SM season.

In the middle and upper troposphere, the BC distribution is governed mainly by the horizontal and vertical advection, but they have opposite effects on BC. The vertical advection brings BC from the lower troposphere into the middle troposphere throughout the year. The magnitude of the horizontal advection is higher compared to the vertical advection in the middle troposphere during WM and MT seasons, and thus, most of the BC is advected horizontally out of the Indian region during these seasons. In contrast, the vertical advection dominates and transports BC further to the upper troposphere during the SM season. The BC tendencies due to the horizontal and vertical advection are of similar magnitude in the upper

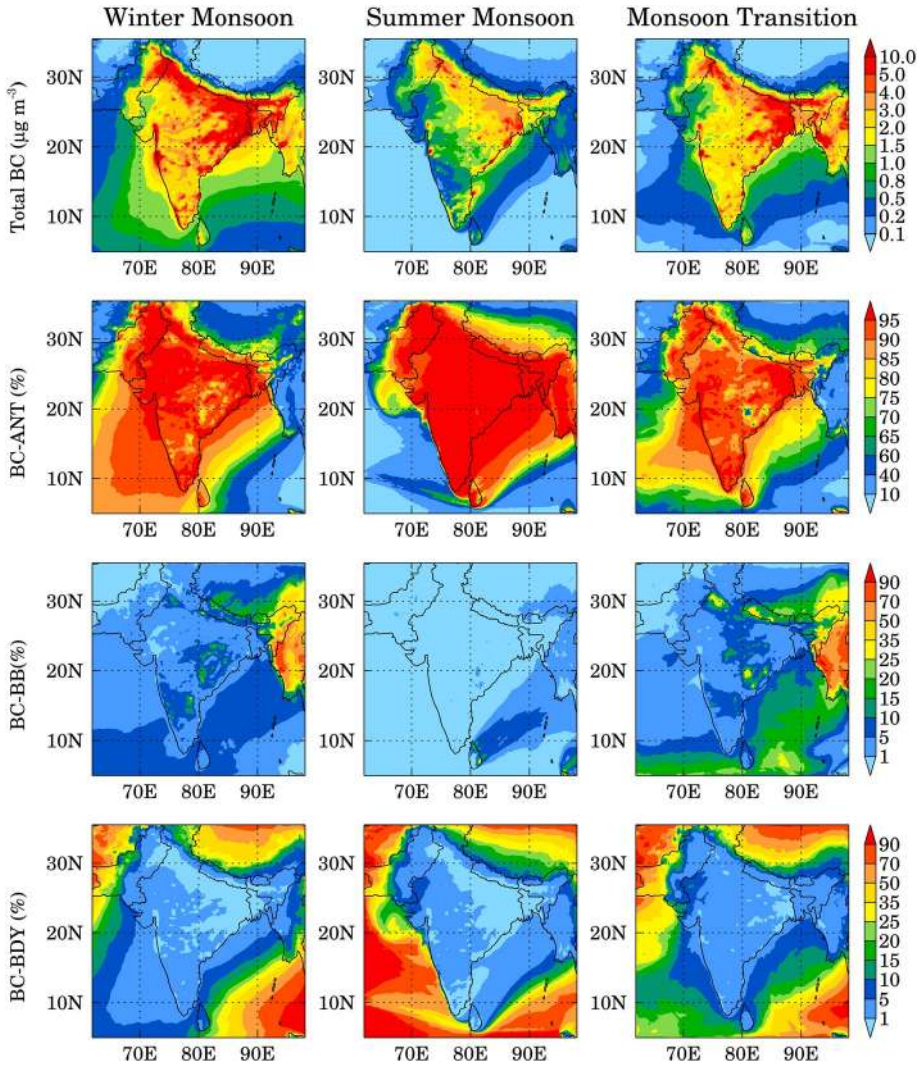

Figure 11. Spatial distributions of the surface layer BC mass concentration over the model domain during WM, SM, and MT seasons. The relative contributions of BC-ANT, BC-BB, and BC-BDY are also shown for each season. Note different color bars for different rows.

troposphere during the WM and MT seasons. However, the combined tendency of the vertical advection and the convective transport is greater than the horizontal advection, indicating that some of the BC could be transported from the upper troposphere to the stratosphere during the SM season.

In summary, the above analysis revealed opposite seasonal cycles of BC in the lower (below 3 km) and free (above 3 km) troposphere. The analysis of BC tracers and tendency terms showed that the summertime minimum in the lower troposphere and the maximum in the free troposphere are not driven by seasonal changes in anthropogenic emissions but by a weakening of the horizontal transport of BC and a strengthening of the vertical transport relative to the winter monsoon.

3.3. Source Contribution Analysis

To identify the most important sources of BC in South Asia, we analyze the spatial distributions of total BC mass concentrations and the relative contributions of anthropogenic (BC-ANT), biomass burning (BC-BB), and boundary inflow (BC-BDY) to the total BC during WM, SM, and MT seasons at the surface (Figure 11) and in the free troposphere (3–15 km; Figure 12). Figure 11 shows that anthropogenic emissions are the most important sources of near surface BC in most parts of South Asia during all seasons. Biomass burning appears as the most important source over Burma and a significant source over other parts of South Asia

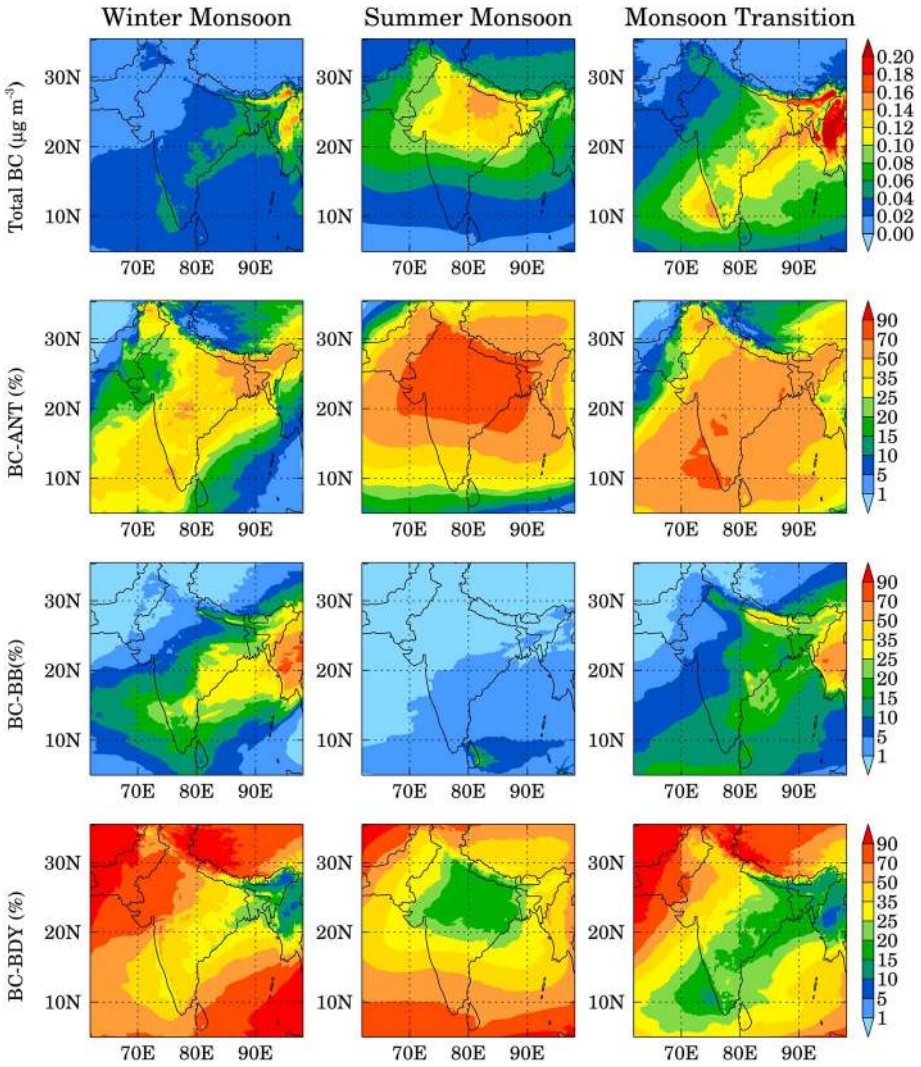

Figure 12. Spatial distributions of free tropospheric (3–15 km) BC mass concentration over the model domain during WM, SM, and MT seasons. The relative contributions of BC-ANT, BC-BB, and BC-BDY are also shown for each season. Note different color bars for different rows.

during the WM and MT seasons. The inflow from domain boundaries is the most important source for the southeast Bay of Bengal during all the seasons and for Arabian Sea during SM and MT seasons. The distributions of total BC mass concentration and relative contribution of different sources in the lower troposphere (0.1–3 km) are very similar to the surface (not shown).

BC mass concentrations in the free troposphere are highest over Burma during WM and MT seasons, and over the eastern Indo-Gangetic Plain and central India during the SM season (Figure 12). The anthropogenic emissions of BC significantly contribute to the BC mass concentrations even in the free troposphere; however, their relative contribution decreases compared to the lower troposphere as BC inflow from the domain boundaries becomes more important. In fact, majority of free tropospheric BC during SM and MT seasons is due to anthropogenic sources. Similar to the lower troposphere, biomass burning is the major source of free tropospheric BC over Burma during WM and MT seasons. Biomass burning also contributes significantly (>25%) to the free tropospheric BC over the northern Bay of Bengal and eastern India during WM and MT seasons.

The contributions of anthropogenic, biomass burning, and boundary inflow to total BC mass concentration at the surface in the lower and free troposphere of the Indian region (68°–91°E, 7°–35°N) during WM, SM, and

Table 2. Average ± Standard Deviation in Mass Concentration (μg m^{-3}) of Total BC, BC From Anthropogenic Sources (BC-ANT), Biomass Burning (BC-BB), and Model Domain Boundaries (BC-BDY) Averaged Over the Indian Region (68°–91°E, 7°–35°N) During WM, SM, and MT Seasons[a]

	Winter Monsoon	Summer Monsoon	Monsoon Transition
		Surface	
Total BC	2.40 ± 2.34	1.02 ± 1.18	1.67 ± 1.80
BC-ANT	2.14 ± 2.20	0.99 ± 1.17	1.41 ± 1.62
BC-BB	0.21 ± 0.25	0.01 ± 0.02	0.21 ± 0.33
BC-BDY	0.06 ± 0.05	0.02 ± 0.02	0.05 ± 0.01
		Lower Troposphere (0–3 km)	
Total BC	1.09 ± 0.78	0.55 ± 0.57	0.88 ± 72
BC-ANT	0.96 ± 0.74	0.52 ± 0.57	0.75 ± 0.66
BC-BB	0.07 ± 0.06	0.01 ± 0.01	0.08 ± 0.08
BC-BDY	0.06 ± 0.04	0.02 ± 0.01	0.05 ± 0.01
		Free Troposphere (3–15 km)	
Total BC	0.027 ± 0.014	0.071 ± 0.038	0.070 ± 0.039
BC-ANT	0.009 ± 0.009	0.049 ± 0.036	0.041 ± 0.029
BC-BB	0.004 ± 0.004	0.001 ± 0.001	0.009 ± 0.009
BC-BDY	0.014 ± 0.004	0.021 ± 0.003	0.020 ± 0.005

[a]The standard deviation was calculated from all the BC values in the Indian region and thus represents the spatial variability of modeled average BC values in South Asia.

MT seasons are given in Table 2. At the surface and in the lower troposphere, anthropogenic emissions contribute about 95–97% of the total BC loading during the SM season, and about 88–89% and 84–85% during WM and MT seasons. Biomass burning sources contribute about 6–9%, 1–2%, and 9–13% during the WM, SM, and MT seasons, respectively. The inflow of BC from domain boundaries contributes only about 2–3% at the surface and 4–6% in the lower troposphere during different seasons. These contributions are compared to those for the March–May 2006 in *Kumar et al.* [2015]. In the free troposphere, the contribution of inflow from domain boundaries becomes significant (27–52%) with the highest contribution during the WM season and the lowest contribution during the SM season. Anthropogenic sources contribute about 60–70% to the free tropospheric BC during SM and MT seasons over the Indian region. The contribution of biomass burning to the free tropospheric BC over the Indian region is not as high as it is over Burma and is about 13–15% during the WM and MT seasons.

3.4. Source-Receptor Relationships and Transport Pathways of BC

It was shown in the previous section that anthropogenic emissions are the main sources of BC not only in the lower troposphere but also in the free troposphere over India. In this section, we examine how seasonal changes in meteorology affect source-receptor relationships among different Indian regions in the lower troposphere and which geographical regions contribute more to anthropogenic BC in the free troposphere of India.

3.4.1. Lower Troposphere

The spatial distributions of BC emitted from anthropogenic sources in North, West, East, and South India during WM, SM, and MT seasons at the surface are shown in Figure 13. The spatial distributions of these BC tracers for the lower troposphere are similar to the surface and thus are not shown. Large seasonal changes in source-receptor relationships are seen as BC is transported from northern to southern parts of India during WM and MT seasons, and from southern to northern parts during the SM season.

BC emitted from North India affects all other parts of India during WM season, and South India plays a similar role during SM season. BC emitted from West India travels mostly to the Arabian Sea and some parts of South and East India during WM season and to North and East India during SM season. BC emitted from East India is transported to the Bay of Bengal, South India, and Arabian Sea during WM season and mostly to North India during SM season. BC emitted from South India is transported mainly to the southern Arabian Sea during WM season and to the Bay of Bengal, and East and North India during SM season. BC emitted from different regions of India during MT season follow transport pathways nearly similar to WM season except that the spatial extent of their influence is smaller compared to the WM season likely because of slower winds (Figure 3). However, BC emitted from South India shows a stronger impact in the Bay of Bengal during MT season.

To quantify the contribution of regional transport to BC loadings in different regions of India, we estimate the contribution of local and regional anthropogenic emissions to total anthropogenic BC loadings in different

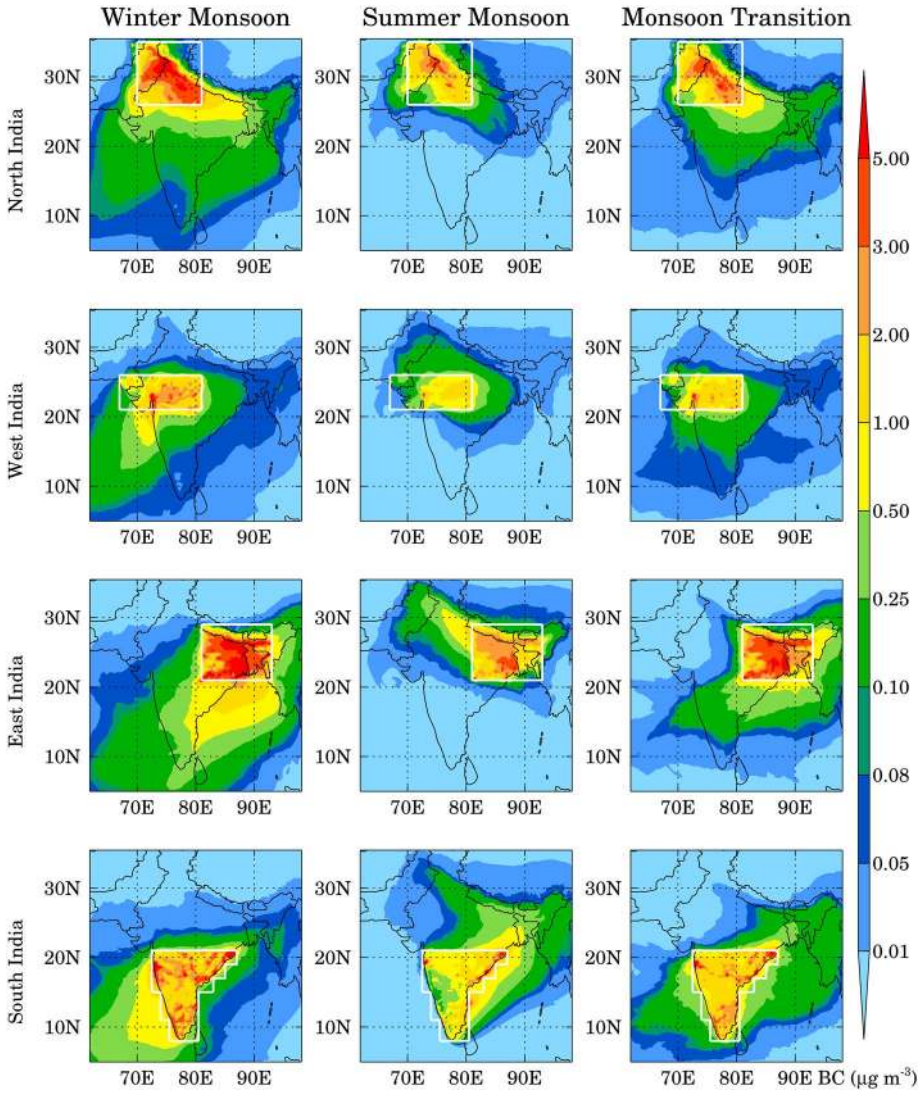

Figure 13. Spatial distribution of anthropogenic BC emitted from North, West, East, and South India during the WM, SM, and MT seasons at the surface. White solid lines mark the geographical boundaries of different regions.

regions (Figure 14). The amount of BC due to sources located in a given region itself (e.g., North India) is defined as the contribution from local sources, and BC coming from sources outside this region (e.g., sum of BC coming from West, East, and South India, and other regions for North India) is defined as the contribution from the regional sources. During WM and MT seasons, local sources contribute about 94–96% to the anthropogenic BC loading in North India, while their contribution ranges from 68% to 81% in West, East, and South India, indicating a significant contribution from regional transport (19–32%). In contrast, local sources dominate anthropogenic BC loadings in South India with a contribution of about 95% during SM season, while regional sources become important for North India with a contribution of about 28%. Regional sources remain important for West and East India during SM season with a contribution of about 26–28%. The local and regional source contributions for the MT season are comparable to those estimated for the March–May 2006 season by *Kumar et al.* [2015], who found that regional sources contribute up to 30% in West India and 25% in East India, respectively, during March–May 2006.

3.4.2. Free Troposphere

To understand the relative importance of anthropogenic emissions from different geographical regions of India, we examined the spatial distribution of BC emitted from anthropogenic sources in North, West, East, and South India in the free troposphere during the WM, SM, and MT seasons (Figure 15). Three features

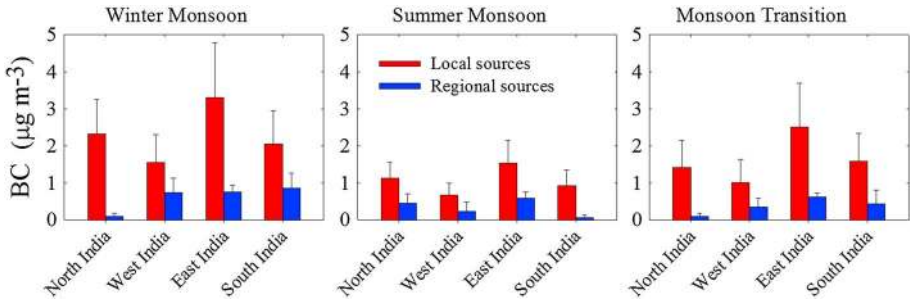

Figure 14. Contribution of local and regional emission sources to anthropogenic BC mass concentration in North, West, East, and South India during WM, SM, and MT seasons of the year 2011.

stand out immediately from Figure 15. First, large seasonal changes are seen in the way BC emitted from different Indian regions affects the free troposphere. Second, the influence of anthropogenic emissions in the free troposphere during WM season is much smaller compared to SM and MT seasons. Third, BC emitted from all the Indian regions affects a large area of free troposphere during the MT seasons.

The largest influence of BC emitted from North India on the free tropospheric BC is seen in eastern India during the WM and MT seasons, and in North and West India during SM season. The influences of BC emitted from North India reached into the free troposphere over the Himalayas, East India, central India, and northern parts of the Bay of Bengal and the Arabian Sea during the SM season, and the influences reach further south during the MT season. BC emitted from the West India has the largest effect on free tropospheric BC in East India during WM, West India during SM, and West and South India during MT season. The East Indian anthropogenic sources generally has the largest effect on the East Indian free tropospheric BC itself, but significant influence reaches in the Himalayas and western part of the Indian subcontinent during the SM season, and in the Bay of Bengal, South India, and the Arabian Sea during WM and MT seasons. The largest influence of BC emitted from South India on the free tropospheric BC is seen in South India during WM season, in East India during SM season, and in South India, the Arabian Sea, and the Bay of Bengal during the MT season. The relative contributions of BC emitted from anthropogenic sources located in North, West, East, and South India, and other regions to the free tropospheric BC mass concentration during WM, SM, and MT seasons are given in Table 3. It is found that the highest contributions to the anthropogenic BC mass concentration in the free troposphere over the Indian region are from the anthropogenic sources located in North and South India during WM and MT seasons, from those located in North, East, and South India during SM season.

4. Summary

This study identifies major processes controlling the seasonal cycle and their relative importance, source-receptor relationship, and transport pathways of near surface black carbon (BC) aerosols over India using a physically consistent and computationally efficient explicit emission tagging technique in WRF-Chem. High resolution (10 km) WRF-Chem simulations are conducted for the year 2011 and evaluated against BC observations for the first time over a network of 21 sites and planetary boundary layer height estimates available at 31 sites in India. WRF-Chem reproduces the observed seasonal cycle of BC fairly well ($0.56 < r < 0.94$) at about 80% (17 out of 21) of the sites considered here but fails to capture seasonality of BC at the sites located in the Himalayan region. A comparison of modeled and observed diurnal variations of BC mass concentrations showed that larger differences between the model and observations occur during nighttime, which could be related to an underestimation of the planetary boundary layer height by WRF-Chem. Other sources of errors in model results include uncertainties in BC emission estimate, errors in parameterization of aerosol processes, model simulated orography and transport processes, boundary conditions from global model, and numerical errors.

WRF-Chem simulated and observed BC in the lower troposphere of India has the highest values during the winter monsoon and the lowest values during the summer monsoon. In contrast, BC in the free troposphere shows an opposite seasonal cycle with the highest values during the summer monsoon and

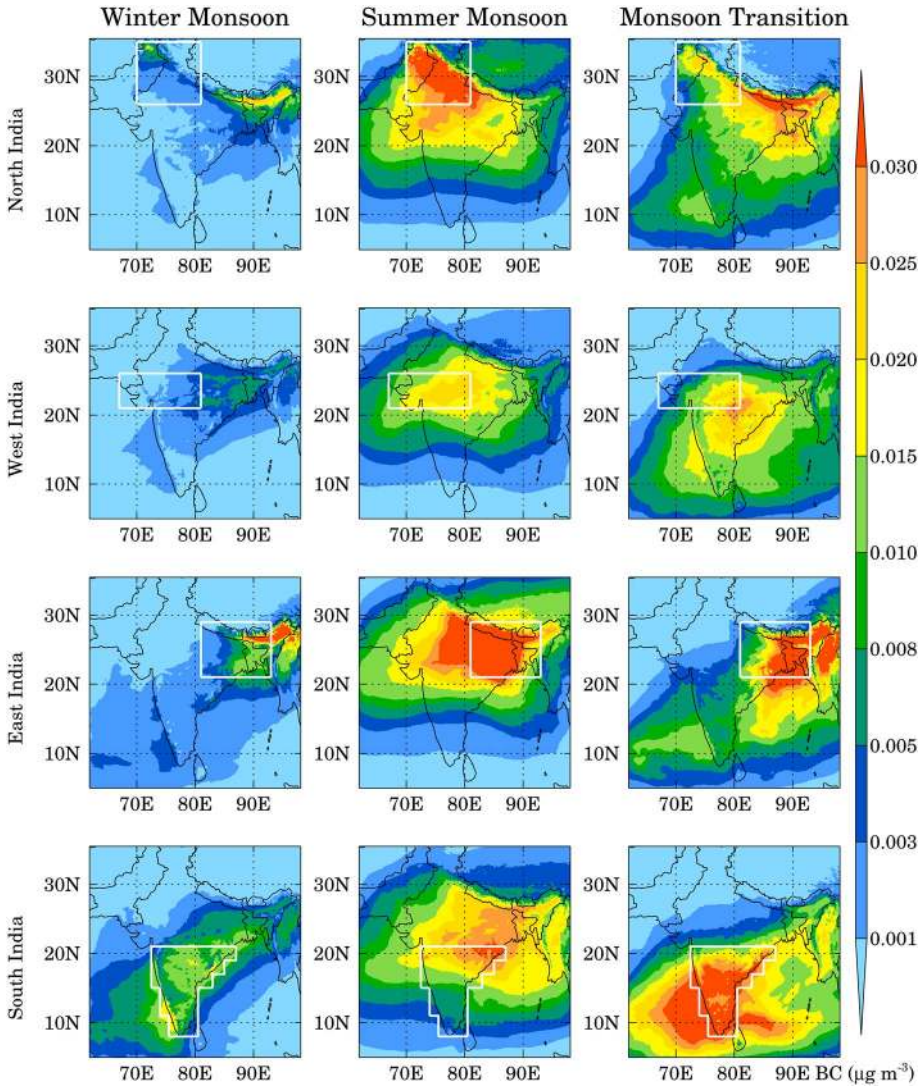

Figure 15. Spatial distribution of anthropogenic BC emitted from North, West, East, and South India during the WM, SM, and MT seasons in the free troposphere. White solid lines mark the geographical boundaries of different regions.

the lowest values during the winter monsoon. We estimate that the seasonality in anthropogenic emissions contributes only 6 ± 10% to the amplitude of the BC seasonal cycle at the surface, suggesting that the seasonal cycle of BC in India is mainly driven by changes in regional meteorology. Model results show that the summertime minimum in the lower troposphere and maximum in the middle and upper troposphere in BC over the Indian region are driven by an increase in the strength of vertical diffusion, convection and advection, and weakening of the horizontal advection during the summer monsoon. In the lower troposphere, anthropogenic emissions account for 84–97% of BC mass concentration in India throughout the year, while open biomass burning emissions contribute a maximum of 9–13% during the winter monsoon and monsoon transition seasons. The inflow of BC from domain boundaries contributes only about 2–3% in the lower troposphere during

Table 3. The Relative Contributions of BC Emitted From Anthropogenic Sources Located in North, West, East, and South India, and Other Regions of the Domain to Free Tropospheric Anthropogenic BC Mass Concentrations Over the Indian Region

	Winter Monsoon	Summer Monsoon	Monsoon Transition
North India	23 ± 20%	26 ± 12%	34 ± 25%
West India	13 ± 7%	14 ± 4%	19 ± 11%
East India	17 ± 10%	26 ± 12%	14 ± 12%
South India	40 ± 21%	29 ± 14%	25 ± 21%
Others	7 ± 9%	5 ± 3%	7 ± 11%

different seasons. The BC inflow from the domain boundaries becomes important in the free troposphere and is the most important source of free tropospheric BC in the Indian region during the winter monsoon, but it is anthropogenic emissions which provide most of the BC loading (60–70%) in the free troposphere during the summer monsoon and monsoon transition seasons.

We find large seasonal changes in source-receptor relationships in both the lower and free troposphere. In the lower troposphere, BC is transported from northern to southern parts of India during winter monsoon and monsoon transition seasons, while from southern to northern parts during the summer monsoon season. Our results demonstrate that regional transport is a key process throughout the year and contributes up to 32% of anthropogenic BC in different regions of India. These results highlight the importance of considering nonlocal sources along with local emissions when designing strategies for mitigating BC impacts related to air quality in this region. However, multi-year and statistical analysis should be performed to lend more confidence in these results. We also find that BC in the free troposphere over the Indian region is affected mostly by the anthropogenic sources located in North and South India during the winter monsoon and monsoon transition seasons, and from those located in North, East, and South India during the summer monsoon season.

While this study has provided important information about the processes controlling the seasonal cycle of black carbon aerosols in atmosphere of the Indian region, several shortcomings of the model were also identified. These include limited ability of the model in reproducing the absolute magnitude and diurnal cycle of BC at several low altitude stations, underestimation of planetary boundary layer height, and failure to capture seasonal cycle of BC in the Himalayas. This indicates that further research efforts are required to improve BC emission estimates, their diurnal variability, and representation of subgrid scale processes. At the same time, it is also imperative to expand the BC observational database to include long-term, systematic, and colocated measurements of vertical distribution, refractory BC mass, mixing state of aerosols and deposition of BC, and relevant meteorological parameters such as planetary boundary layer height for further model evaluation.

Acknowledgments

We thank L. Emmons and S. Tilmes for their constructive suggestions on the manuscript. The data sets of initial and boundary conditions for meteorological fields are downloaded from http://dss.ucar.edu/datasets/ds113.0. The data sets for initial and boundary conditions for chemical fields, biomass burning emissions, and programs used to process these data sets are downloaded from the website http://www2.acd.ucar.edu/wrf-chem/. Anthropogenic emission data set is obtained from EC-JRC/PBL, EDGAR version 4.2 (http://edgar.jrc.ec.europa.eu/). We thank NOAA for providing PBLH data sets as a part of the Integrated Global Radiosonde Archive (http://www.ncdc.noaa.gov/data-access/weather-balloon/integrated-global-radiosonde-archive). Data used to obtain the results of this paper can be obtained by contacting Rajesh Kumar (rkumar@ucar.edu). The National Center for Atmospheric Research is supported by the National Science Foundation. Comments from three anonymous reviewers are greatly appreciated.

References

Adhikary, B., G. R. Carmichael, Y. Tang, L. R. Leung, Y. Qian, J. J. Schauer, E. A. Stone, V. Ramanathan, and M. V. Ramana (2007), Characterization of the seasonal cycle of South Asian aerosols: A regional-scale modeling analysis, *J. Geophys. Res.*, *112*, D22S22, doi:10.1029/2006JD008143.

Arnott, W. P., K. Hamasha, H. Moosmuller, P. J. Sheridan, and J. A. Ogren (2005), Towards aerosol light-absorption measurements with a 7-wavelength aethalometer: Evaluation with a photoacoustic instrument and 3-wavelength nephelometer, *Aerosol Sci. Technol.*, *39*, 17–29, doi:10.1080/027868290901972.

Asnani, G. C. (2005), Climatology of the tropics, in *Tropical Meteorology*, vol. 1, pp. 100–204, Praveen Printing Press, Pune, India.

Babu, S. S. and K. K. Moorthy (2002), Aerosol black carbon over a tropical coastal station in India, *Geophys. Res. Lett.*, *29*(23), 2098, doi:10.1029/2002GL015662.

Barth, M. C., and A. T. Church (1999), Regional and global distributions and lifetimes of sulfate aerosols from Mexico City and southeast China, *J. Geophys. Res.*, *104*(D23), 30,231–30,239, doi:10.1029/1999JD900809.

Barth, M. C., J. Lee, A. Hodzic, G. Pfister, W. C. Skamarock, J. Worden, J. Wong, and D. Noone (2012), Thunderstorms and upper troposphere chemistry during the early stages of the 2006 North American Monsoon, *Atmos. Chem. Phys.*, *12*, 11,003–11,026, doi:10.5194/acp-12-11003-2012.

Bond, T. C., E. Bhardwaj, R. Dong, R. Jogani, S. Jung, C. Roden, D. G. Streets, and N. M. Trautmann (2007), Historical emissions of black and organic carbon aerosol from energy related combustion, 1850–2000, *Global Biogeochem. Cycles*, *21*, GB2018, doi:10.1029/2006GB002840.

Bond, T. C., et al. (2013), Bounding the role of black carbon in the climate system: A scientific assessment, *J. Geophys. Res. Atmos.*, *118*, 1–173, doi:10.1002/jgrd.50171.

Chameides, W. L., et al. (1999), Case study of the effects of atmospheric aerosols and regional haze on agriculture: An opportunity to enhance crop yields in China through emission controls, *Proc. Natl. Acad. Sci. U.S.A.*, *96*, 13,626–13,633.

Chin, M., R. B. Rood, S.-J. Lin, J.-F. Müller, and A. M. Thompson (2000), Atmospheric sulfur cycle simulated in the global model GOCART: Model description and global properties, *J. Geophys. Res.*, *105*(D20), 24,671–24,687, doi:10.1029/2000JD900384.

Chin, M., P. Ginoux, S. Kinne, O. Torres, B. N. Holben, B. N. Duncan, R. V. Martin, J. A. Logan, A. Higurashi, and T. Nakajima (2002), Tropospheric aerosol optical thickness from the GOCART model and comparisons with satellite and sun photometer measurements, *J. Atmos. Sci.*, *59*, 461–483.

Chou, M.–. D., and M. J. Suarez (1994), An efficient thermal infrared radiation parameterization for use in general circulation models *NASA Tech. Memo*, 84 pp.

Dockery, D. W., and P. H. Stone (2007), Cardiovascular risks from fine particulate air pollution, *N. Engl. J. Med.*, *365*, 511–513.

Dumka, U. C., K. K. Moorthy, R. Kumar, P. Hegde, R. Sagar, P. Pant, N. Singh, and S. S. Babu (2010), Characteristics of aerosol black carbon mass concentration over a high altitude location in the Central Himalayas from multi-year measurements, *Atmos. Res.*, *96*(4), 510–521.

Dumka, U. C., R. K. Manchanda, P. R. Sinha, S. Sreenivasan, K. K. Moorthy, and S. S. Babu (2013), Temporal variability and radiative impact of black carbon aerosol over tropical urban station Hyderabad, *J. Atmos. Sol. Terr. Phys.*, *105–106*, 81–90.

Durre, I., and X. Yin (2008), Enhanced radiosonde data for studies of vertical structure, *Bull. Am. Meteorol. Soc.*, *89*, 1257–1262, doi:10.1175/2008BAMS2603.1.

Durre, I., R. S. Vose, and D. B. Wuertz (2006), Overview of the Integrated Global Radiosonde Archive, *J. Clim.*, *19*, 53–68, doi:10.1175/JCLI3594.1.

Emmons, L. K., et al. (2010), Description and evaluation of the Model for Ozone and Related chemical Tracers, version 4 (MOZART-4), *Geosci. Model Dev.*, *3*, 43–67, doi:10.5194/gmd-3-43-2010.

Fadnavis, S., et al. (2013), Transport of aerosols into the UTLS and their impact on the Asian monsoon region as seen in a global model simulation, *Atmos. Chem. Phys.*, *13*, 8771–8786, doi:10.5194/acp-13-8771-2013.

Fadnavis, S., M. G. Schultz, K. Semeniuk, A. S. Mahajan, L. Pozzoli, S. Sonbawne, S. D. Ghude, M. Kiefer, and E. Eckert (2014), Trends in peroxyacetyl nitrate (PAN) in the upper troposphere and lower stratosphere over southern Asia during the summer monsoon season: Regional impacts, *Atmos. Chem. Phys.*, *14*, 12,725–12,743, doi:10.5194/acp-14-12725-2014.

Forbes, M. S., R. J. Raison, and J. O. Skjemstad (2006), Formation, transformation and transport of black carbon (charcoal) in terrestrial and aquatic ecosystems, *Sci. Total Environ.*, *370*, 190–206.

Freitas, S. R., K. M. Longo, R. Chatfield, D. Latham, M. A. F. Silva Dias, M. O. Andreae, E. Prins, J. C. Santos, R. Gielow, and J. A. Carvalho Jr. (2007), Including the sub-grid scale plume rise of vegetation fires in low resolution atmospheric transport models, *Atmos. Chem. Phys.*, *7*, 3385–3398, doi:10.5194/acp-7-3385-2007.

Ghude, S. D., G. G. Pfister, C. Jena, R. J. van der A, L. K. Emmons, and R. Kumar (2013), Satellite constraints of nitrogen oxide (NOx) emissions from India based on OMI observations and WRF-Chem simulations, *Geophys. Res. Lett.*, *40*, 423–428, doi:10.1029/2012GL053926.

Ghude, S. D., C. Jena, D. M. Chate, G. Beig, G. G. Pfister, R. Kumar, and V. Ramanathan (2014), Reductions in India's crop yield due to ozone, *Geophys. Res. Lett.*, *41*, 5685–5691, doi:10.1002/2014GL060930.

Girach, I. A., and P. R. Nair (2014), Carbon monoxide over Indian region as observed by MOPITT, *Atmos. Environ.*, *99*, 599–609, doi:10.1016/j.atmosenv.2014.10.019.

Gogoi, M. M., S. S. Babu, K. K. Moorthy, M. R. Manoj, and J. P. Chaubey (2013), Absorption characteristics of aerosols over the northwestern region of India: Distinct seasonal signatures of biomass burning aerosols and mineral dust, *Atmos. Environ.*, *73*, 92–102.

Grell, G., and A. D. Devenyi (2002), A generalized approach to parameterizing convection combining ensemble and data assimilation techniques. *Geophys. Res. Lett.*, *29*(14), 1693, doi:10.1029/2002GL015311.

Grell, G. A., S. E. Peckham, R. Schmitz, S. A. McKeen, G. Frost, W. C. Skamarock, and B. Eder (2005), A fully coupled "online" chemistry within the WRF model, *Atmos. Environ.*, *39*, 6957–6975.

Guha, A., B. K. De, P. Dhar, T. Banik, M. Chakraborty, R. Roy, A. Choudhury, M. M. Gogoi, S. Suresh Babu, and K. Krishna Moorthy (2015), Seasonal characteristics of aerosol black carbon in relation to long range transport over Tripura in Northeast India, *Aerosol Air Qual. Res.*, *15*(3), 786–798, doi:10.4209/aaqr.2014.02.0029.

Hansen, A. D. A., H. Rosen, and T. Novakov (1984), The aethalometer, an instrument for the real-time measurement of optical absorption by aerosol particles, *Sci. Total Environ.*, *36*, 191–196, doi:10.1016/0048-9697(84)90265-1.

Hansen, J., M. Sato, and R. Ruedy (1997), Radiative forcing and climate response, *J. Geophys. Res.*, *102*(D6), 6831–6864, doi:10.1029/96JD03436.

He, C., et al. (2014), A global 3-D CTM evaluation of black carbon in the Tibetan Plateau, *Atmos. Chem. Phys.*, *14*, 7091–7112, doi:10.5194/acp-14-7091-2014.

Henriksson, S. V., A. Laaksonen, V. M. Kerminen, P. Räisänen, H. Järvinen, A. M. Sundström, and G. de Leeuw (2011), Spatial distributions and seasonal cycles of aerosols in India and China seen in global climate aerosol model, *Atmos. Chem. Phys.*, *11*, 7975–7990, doi:10.5194/acp-11-7975-2011.

Hong, S.–. Y., Y. Noh, and J. Dudhia (2006), A new vertical diffusion package with an explicit treatment of entrainment processes, *Mon. Weather Rev.*, *134*, 2318–2341.

Jacobson, M. (2001), Strong radiative heating due to the mixing state of BC in atmospheric aerosols, *Nature*, *409*, 695–697.

Jacobson, M. (2004), Climate response of fossil fuel and biofuel soot accounting for soot's feedback to snow and sea ice albedo and emissivity, *J. Geophys. Res.*, *109*, D21201, doi:10.1029/2004JD004945.

Janseen, N. A. H., M. E. Gerlofs-Nijland, T. Lanki, R. O. Salonen, F. Cassee, G. Hoek, P. Fischer, B. Brunekreef, and M. Krzyzanowski (2012), *Health Effects of Black Carbon*, pp. 1–96, World Health Organization, Copenhagen, Denmark.

Janssens-Maenhout, G., et al. (2015), HTAP_v2: A mosaic of regional and global emission gridmaps for 2008 and 2010 to study hemispheric transport of air pollution, *Atmos. Chem. Phys. Discuss.*, *15*, 12,867–12,909, doi:10.5194/acpd-15-12867-2015.

Jena, C., S. D. Ghude, G. G. Pfister, D. M. Chate, R. Kumar, G. Beig, D. Surendran, S. Fadnavis, and D. M. Lal (2014), Influence of springtime biomass burning emissions in South Asia on regional ozone: A model based case study, *Atmos. Environ.*, *100*, 37–47, doi:10.1016/j.atmosenv.2014.10.027.

Jimenez, P., R. Parra, S. Gasso, and J. M. Baldasano (2005), Modeling the ozone weekend effect in very complex terrains: A case study in the Northeastern Iberian Peninsula, *Atmos. Environ.*, *39*(3), 429–444.

Joshi, H., M. Naja, K. P. Singh, R. Kumar, P. Bhardwaj, S. S. Babu, S. K. Satheesh, K. K. Moorthy, and H. C. Chandola (2014), Investigation of aerosol black carbon from a semi-urban site in the Indo-Gangetic Plain, *Atmos. Environ.*, doi:10.1016/j.atmosenv.2015.04.007.

Kanawade, V. P., S. N. Tripathi, D. Bhattu, and P. M. Shamjad (2014), Sub-micron particle number size distributions characteristics at an urban location, Kanpur, in the Indo-Gangetic Plain, *Atmos. Res.*, *147–148*, 121–132.

Kant, Y., P. Patel, A. K. Mishra, U. C. Dumka, and V. K. Dadhwal (2012), Diurnal and seasonal aerosol optical depth and black carbon in the Shiwalik hills of the north western Himalayas: A case study of the Doon Valley, India, *Int. J. Geol. Earth Environ. Sci.*, *2*, 173–192.

Koch, D., and A. D. Del Genio (2010), Black carbon semi-direct effects on cloud cover: Review and synthesis, *Atmos. Chem. Phys.*, *10*, 7685–7696, doi:10.5194/acp-10-7685-2010.

Kompalli, S. K., S. S. Babu, K. K. Moorthy, M. R. Manoj, N. V. P. Kiran Kumar, K. Hareef Baba Shaeb, and A. K. Joshi (2014), Aerosol black carbon characteristics over central India: Temporal variation and its dependence on mixed layer height, *Atmos. Res.*, *147–148*, 27–37.

Kumar, R., M. Naja, G. G. Pfister, M. C. Barth, and G. P. Brasseur (2012a), Simulations over South Asia using the Weather Research and Forecasting Model with Chemistry (WRF-Chem): Set-up and meteorological evaluation, *Geosci. Model Dev.*, *5*, 321–343, doi:10.5194/gmd-5-321-2012.

Kumar, R., M. Naja, G. G. Pfister, M. C. Barth, C. Wiedinmyer, and G. P. Brasseur (2012b), Simulations over South Asia using the Weather Research and Forecasting Model with Chemistry (WRF-Chem): Chemistry evaluation and initial results, *Geosci. Model Dev.*, *5*, 619–648, doi:10.5194/gmd-5-619-2012.

Kumar, R., M. Naja, G. G. Pfister, M. C. Barth, and G. P. Brasseur (2013), Source attribution of carbon monoxide in India and surrounding regions during wintertime, *J. Geophys. Res. Atmos.*, *118*, 1981–1995, doi:10.1002/jgrd.50134.

Kumar, R., M. C. Barth, G. G. Pfister, M. Naja, and G. P. Brasseur (2014a), WRF-Chem simulations of a typical pre-monsoon dust storm in northern India: Influences on aerosol optical properties and radiation budget, *Atmos. Chem. Phys.*, *14*, 2431–2446, doi:10.5194/acp-14-2431-2014.

Kumar, R., M. C. Barth, S. Madronich, M. Naja, G. R. Carmichael, G. G. Pfister, C. Knote, G. P. Brasseur, N. Ojha, and T. Sarangi (2014b), Effects of dust aerosols on tropospheric chemistry during a typical pre-monsoon season dust storm in northern India, *Atmos. Chem. Phys.*, *14*, 6813–6834, doi:10.5194/acp-14-6813-2014.

Kumar, R., M. Barth, V. S. Nair, G. Pfister, S. Suresh Babu, S. K. Satheesh, K. Krishna Moorthy, G. R. Carmichael, Z. Lu, and D. G. Streets (2015), Sources of black carbon aerosols in South Asia and surrounding regions during the Integrated Campaign for Aerosols, Gases and Radiation Budget (ICARB), *Atmos. Chem. Phys.*, *15*, 5415–5428, doi:10.5194/acp-15-5415-2015.

Lau, K. M., M. K. Kim, and K. M. Kim (2006), Asian summer monsoon anomalies induced by aerosol direct forcing: The role of the Tibetan Plateau, *Clim. Dyn.*, *26*, 855–864, doi:10.1007/s00382-006-0114-z.

Lau, W. K. M., and K. M. Kim (2010), Fingerprinting the impacts of aerosols on long-term trends of the Indian summer monsoon region rainfall, *Geophys. Res. Lett.*, *37*, L16705, doi:10.1029/2010GL043255.

Lawrence, M. G., and J. Lelieveld (2010), Atmospheric pollutants outflow from southern Asia: A review, *Atmos. Chem. Phys.*, *10*, 11,017–11,096, doi:10.5194/acp-10-11017-2010.

Lelieveld, J., et al. (2001), The Indian Ocean experiment: Widespread air pollution from South and Southeast Asia, *Science*, *291*, 1031–1036.

Liu, J., S. Fan, L. W. Horowitz, and H. Levy II (2011), Evaluation of factors controlling long-range transport of black carbon to the Arctic, *J. Geophys. Res.*, *116*, D04307, doi:10.1029/2010JD015145.

Lu, Z., Q. Zhang, and D. G. Streets (2011), Sulfur dioxide and primary carbonaceous aerosol emissions in China and India, 1996–2010, *Atmos. Chem. Phys.*, *11*, 9839–9864, doi:10.5194/acp-11-9839-2011.

Mahapatra, P. S., S. Panda, N. Das, S. Rath, and T. Das (2014), Variation in black carbon mass concentration over an urban site in the eastern coastal plains of the Indian sub-continent, *Theor. Appl. Climatol.*, *117*, 133–147, doi:10.1007/s00704-013-0984-z.

Menon, S., J. Hansen, L. K. Nazaren, and Y. Leo (2002), Climate effects of BC aerosols in China and India, *Science*, *297*(5590), 2250–2253.

Menon, S., D. Koch, G. Beig, S. Sahu, J. Fasullo, and D. Orlikowski (2010), Black carbon aerosols and the third polar ice cap, *Atmos. Chem. Phys.*, *10*, 4559–4571, doi:10.5194/acp-10-4559-2010.

Michael, M., A. Yadav, S. N. Tripathi, V. P. Kanawade, A. Gaur, P. Sadavarte, and C. Venkataraman (2014), Simulation of trace gases and aerosols over the Indian domain: Evaluation of the WRF-Chem model, *Geosci. Model Dev. Discuss.*, *7*, 431–482, doi:10.5194/gmdd-7-431-2014.

Mlawer, E. J., S. J. Taubman, P. D. Brown, M. J. Iacono, and S. A. Clough (1997), Radiative transfer for inhomogeneous atmospheres: RRTM, a validated correlated-k model for the longwave, *J. Geophys. Res.*, *102*(D14), 16,663–16,682, doi:10.1029/97JD00237.

Moorthy, K. K., and S. S. Babu (2006), Aerosol black carbon over Bay of Bengal observed from an island location, Port Blair: Temporal features and long-range transport, *J. Geophys. Res.*, *111*, D17205, doi:10.1029/2005JD006855.

Moorthy, K. K., S. N. Beegum, N. Srivastava, S. K. Satheesh, M. Chin, N. Blond, S. S. Babu, and S. Singh (2013), Performance evaluation of chemistry transport models over India, *Atmos. Environ.*, *71*, 210–225.

Nair, A. V., K. M. Kumar, and S. K. Satheesh (2010), Measurements of aerosol black carbon at an urban site in southern India *Proceedings of IASTA-2010 conference*, March 24–26, Darjeeling. [Available at http://www.iasta.org.in/iasta2010dat/session-F1.asp#F-P-7.]

Nair, S., G. Srinivasan, and R. Nemani (2009), Evaluation of multi-satellite TRMM derived rainfall estimates over a western state of India, *J. Meteorol. Soc. Jpn.*, *87*, 927–939, doi:10.2151/jmsj.87.927.

Nair, V. S., S. S. Babu, and K. K. Moorthy (2008), Aerosol characteristics in the marine atmospheric boundary layer over the Bay of Bengal and Arabian Sea during ICARB: Spatial distribution and latitudinal gradients, *J. Geophys. Res.*, *113*, D15208, doi:10.1029/2008JD009823.

Nair, V. S., F. Solmon, F. Giorgi, L. Mariotti, S. S. Babu, and K. K. Moorthy (2012), Simulation of South Asian aerosols for regional climate studies, *J. Geophys. Res.*, *117*, D04209, doi:10.1029/2011JD016711.

Nair, V. S., S. S. Babu, K. K. Moorthy, A. K. Sharma, and A. M. Ajai (2013), Black carbon aerosols over the Himalayas: Direct and surface albedo forcing, *Tellus B*, *65*, 19738, doi:10.3402/tellusb.v65i0.19738.

Olivier, J., J. Peters, C. Granier, G. Pétron, J. F. Müller, and S. Wallens (2003), Present and future surface emissions of atmospheric compounds *POET Rep.*, *2*, EU project EVK2-1999-00011.

Pandey, A., P. Sadavarte, A. B. Rao, and C. Venkataraman (2014), Trends in multi-pollutant emissions from a technology-linked inventory for India: II. Residential, agricultural and informal industry sectors, *Atmos. Environ.*, *99*, 341–352, doi:10.1016/j.atmosenv.2014.09.080.

Pathak, B., G. Kalita, K. Bhuyan, P. K. Bhuyan, and K. K. Moorthy (2010), Aerosol temporal characteristics and its impact on shortwave radiative forcing at a location in the northeast of India, *J. Geophys. Res.*, *115*, D19204, doi:10.1029/2009JD013462.

Pöschl, U. (2005), Atmospheric aerosols: Composition, transformation, climate and health effects, *Angew. Chem., Int. Ed.*, *44*, 7520–7540.

Rakesh, V., R. Singh, and P. C. Joshi (2009), Intercomparison of the performance of MM5/WRF with and without satellite data assimilation in short-range forecast applications over the Indian region, *Meteorol. Atmos. Phys.*, *105*, 133–155, doi:10.1007/s00703-009-0038-3.

Ramachandran, S., and S. Kedia (2010), Black carbon aerosols over an urban region: Radiative forcing and climate impact, *J. Geophys. Res.*, *115*, D10202, doi:10.1029/2009JD013560.

Ramanathan, V., and G. Carmichael (2008), Global and regional climate changes due to black carbon, *Nat. Geosci.*, *1*, 221–227.

Ramanathan, V., et al. (2001), Indian Ocean experiment: An integrated analysis of the climate forcing and effects of great Indio-Asian haze, *J. Geophys. Res.*, *106*(D22), 28,371–28,398, doi:10.1029/2001JD900133.

Ramanathan, V., C. Chung, D. Kim, T. Bettge, L. Buja, J. T. Kiehl, W. M. Washington, Q. Fu, D. R. Sikka, and M. Wild (2005), Atmospheric brown clouds: Impacts on South Asian climate and hydrological cycle, *Proc. Natl. Acad. Sci. U.S.A.*, *102*(15), 5326–5333.

Ratnam, V. J., and K. K. Kumar (2005), Sensitivity of the simulated monsoon of 1987 and 1988 to convective parameterization schemes in MM5, *J. Clim.*, *18*, 2724–2743.

Reddy, B. S. K., K. Raghavendra Kumar, G. Balakrishnaiah, K. Rama Gopal, R. R. Reddy, L. S. S. Reddy, Y. Nazeer Ahammed, K. Narasimhulu, K. K. Moorthy, and S. S. Babu (2012), Potential source regions contributing to seasonal variations of black carbon aerosols over Anantapur in Southeast India, *Aerosol. Air Qual. Res.*, *12*, 344–358, doi:10.4209/aaqr.2011.10.

Riemer, N., M. West, R. Zaveri, and R. Easter (2010), Estimating black carbon aging time-scales with a particle resolved aerosol model, *Aero. Sci.*, *41*, 143–158, doi:10.1016/j.jaerosci.2009.08.009.

Sadavarte, P., and C. Venkataraman (2014), Trends in multi-pollutant emissions from a technology-linked inventory for India: I. Industry and transport sectors, *Atmos. Environ.*, *99*, 353–364, doi:10.1016/j.atmosenv.2014.09.081.

Safai, P. D., M. P. Raju, K. B. Budhavant, P. S. P. Rao, and P. C. S. Devara (2013), Long term studies on characteristics of black carbon aerosols over a tropical urban station Pune, India, *Atmos. Res.*, *132–133*, 173–184.

Satheesh, S. K., and V. Ramanathan (2000), Large differences in tropical aerosol forcing at the top of the atmosphere and Earth's surface, *Nature*, *405*, 60–62.

Seidel, D. J., C. O. Ao, and K. Li (2010), Estimating climatological planetary boundary layer heights from radiosonde observations: Comparison of methods and uncertainty analysis, *J. Geophys. Res.*, *115*, D16113, doi:10.1029/2009JD013680.

Sharma, P., J. C. Kuniyal, K. Chand, R. P. Guleria, P. P. Dhyani, and C. Chauhan (2013), Surface ozone concentration and its behaviour with aerosols in the northwestern Himalaya, India, *Atmos. Environ.*, *71*, 44–53.

Skamarock, W. C., J. B. Klemp, J. Dudhia, D. O. Gill, D. M. Barker, M. G. Duda, X.-Y. Huang, W. Wang, and J. G. Powers (2008), A description of the advanced research WRF version 2 NCAR Tech. Note, *NCAR/TN-468+STR*, *Natl. Cent. for Atmos. Res.*, Boulder, Colo.

Surendran, D. E., G. Beig, S. D. Ghude, A. S. Panicker, M. G. Manoj, D. M. Chate, and K. Ali (2013), Radiative forcing of black carbon over Delhi, *Int. J. Photoenergy*, 313652, doi:10.1155/2013/313652.

Tewari, M., F. Chen, W. Wang, J. Dudhia, M. A. LeMone, K. Mitchell, M. Ek, G. Gayno, J. Wegiel, and R. H. Cuenca (2004), Implementation and verification of the unified NOAH land surface model in the WRF model, *20th Conference on Weather analysis and Forecasting/16th Conference on Numerical Weather Prediction*, pp. 11–15.

Thompson, G., R. M. Rasmussen, and K. Manning (2008), Explicit forecasts of winter precipitation using an improved bulk microphysics scheme. Part I: Description and sensitivity analysis, *Mon. Weather Rev.*, *132*, 519–542.

Tiwari, S., A. K. Srivastava, D. S. Bisht, P. Parmita, M. K. Srivastava, and S. D. Attri (2013), Diurnal and seasonal variations of black carbon and PM2.5 over New Delhi, India: Influence of meteorology, *Atmos. Environ.*, *125–126*, 50–62.

Udayasoorian, C., R. M. Jayabalakrishnan, A. R. Suguna, M. M. Gogoi, and S. S. Babu (2014), Aerosol black carbon characteristics over a high altitude Western Ghats location in Southern India, *Ann. Geophys.*, *32*, 1361–1371, doi:10.5194/angeo-32-1361-2014.

Vinoj, V., S. K. Satheesh, and K. K. Moorthy (2008), Aerosol characteristics at a remote island: Minicoy in southern Arabian Sea, *J. Earth Syst. Sci.*, *117*(S1), 389–397.

Walcek, C. J., R. A. Brost, J. S. Chang, and M. L. Wesely (1986), SO_2, sulfate and HNO_3 deposition velocities computed using regional landuse and meteorological data, *Atmos. Environ.*, *20*(5), 949–964.

Wang, H., P. J. Rasch, R. C. Easter, B. Singh, R. Zhang, P.-L. Ma, Y. Qian, S. J. Ghan, and N. Beagley (2014), Using an explicit emission tagging method in global modeling of source-receptor relationships for black carbon in the Arctic: Variations, sources, and transport pathways, *J. Geophys. Res. Atmos.*, *119*, 12,888–12,909, doi:10.1002/2014JD022297.

Wesely, M. L. (1989), Parameterization of surface resistance to gaseous dry deposition in regional-scale numerical models, *Atmos. Environ.*, *23*, 1293–1304.

Wiedinmyer, C., S. K. Akagi, R. J. Yokelson, L. K. Emmons, J. A. Al-Saadi, J. J. Orlando, and A. J. Soja (2011), The Fire INventory from NCAR (FINN): A high resolution global model to estimate the emissions from open burning, *Geosci. Model Dev.*, *4*, 625–641, doi:10.5194/gmd-4-625-2011.

Yasunari, T. J., P. Bonasoni, P. Laj, K. Fujita, E. Vuillermoz, A. Marinoni, P. Cristofanelli, R. Duchi, G. Tartari, and K.-M. Lau (2010), Estimated impact of black carbon deposition during pre-monsoon season from Nepal Climate Observatory-Pyramid data and snow albedo changes over Himalayan glaciers, *Atmos. Chem. Phys.*, *10*, 6603–6615, doi:10.5194/acp-10-6603-2010.

Zaveri, R. A., R. C. Easter, J. D. Fast, and L. K. Peters (2008), Model for simulating aerosol interactions and chemistry (MOSAIC), *J. Geophys. Res.*, *113*, D13204, doi:10.1029/2007JD008782.